Quantum fluctuations and soliton generation in stimulated Raman scattering
by David Clyde MacPherson

A thesis submitted in partial fulfillment of the requirements for the degree of Doctor of Philosophy in Physics
Montana State University

Abstract:
Theoretical and experimental details of initiating and amplifying a Stokes pulse using stimulated Raman scattering in H2 are presented. Statistics associated with the spectral fluctuations of a Stokes seed pulse have been measured and theoretically calculated. The spectral fluctuations are shown to result from quantum noise associated with spontaneous initiation. These spectral fluctuations are an example of an easily measurable macroscopic fluctuation of quantum origin. The effects of frequency fluctuations on the generation of solitons in the nonlinear regime of stimulated Raman scattering are calculated and measured.

A detailed derivation of the fully quantum mechanical stimulated Raman scattering equations is given along with their solution for various approximations. The driven Maxwell's equation for the Raman system is derived from the system Hamiltonian. For treating the quantum initiation of stimulated Raman scattering, the radiation field is expanded in localized coherent modes. The details of calculating and using these modes to generate an ensemble of Stokes pulses are presented along with specific examples and ensemble average statistics. The use of localized modes for treating the pulsed cavityless Raman laser gives insight into the spontaneous initiation of Stokes pulses.

A numerical treatment of soliton initiation and formation in stimulated Raman scattering using a π phase shift is given. The π phase shift is produced in the Stokes seed by modulating its envelope through zero. It is found that by modulating the envelope slowly compared to the coherence decay time, T2, a soliton pulse is initiated which narrows to be much shorter than T2 Our calculations also confirm the prediction that solitons initiated using an off resonance seed decay during formation.

Solitons have also been observed in the pump and Stokes pulses from a Raman generator. It was predicted that solitons would form in the generator due to random phase shifts caused by quantum initiation. We have confirmed these predictions and measured the amplitude distribution of the spontaneous solitons.

QUANTUM FLUCTUATIONS AND SOLITON GENERATION IN STIMULATED RAMAN SCATTERING

by

David Clyde MacPherson

A thesis submitted in partial fulfillment
of the requirements for the degree

of

Doctor of Philosophy

in

Physics

MONTANA STATE UNIVERSITY
Bozeman, Montana

May 1989

APPROVAL

of a thesis submitted by

David Clyde MacPherson

This thesis has been read by each member of the thesis committee and has been found to be satisfactory regarding content, English usage, format, citations, bibliographic style, and consistency, and is ready for submission to the College of Graduate Studies.

5-12-89

Date

Chairperson, Graduate Committee

Approved for the Major Department

5-12-89

Date

Head, Major Department

Approved for the College of Graduate Studies

June 9, 1989

Date

Henry L Parsons

Graduate Dean

STATEMENT OF PERMISSION TO USE

In presenting this thesis in partial fulfillment of the requirements for a doctoral degree at Montana State University, I agree that the Library shall make it available to borrowers under rules of the Library. I further agree that copying of this thesis is allowable only for scholarly purposes, consistent with "fair use" as prescribed in the U.S. Copyright Law. Requests for extensive copying or reproduction of this thesis should be referred to University Microfilms International, 300 North Zeeb Road, Ann Arbor, Michigan 48106, to whom I have granted "the exclusive right to reproduce and distribute copies of the dissertation in and from microfilm and the right to reproduce and distribute by abstract in any format."

Signature David MacPherson

Date 6/22/89

ACKNOWLEDGMENTS

I feel very fortunate to have had Dr. John Carlsten for my thesis adviser. I would like to thank John for making graduate school an enjoyable part of life and for the many hours of stimulating discussions on fundamental physics. I am also greatly indebted to my wife, Susie, for filling my big lunch bag every morning and for her many hours spent typing this thesis.

The help of Rand Swanson and Phil Battle in carefully working through and pointing out errors in my math is greatly appreciated. If there are any errors left, I will blame them. It has been great fun working with Rand Swanson and Jeff Rifkin to solve the various experimental and theoretical problems that came about during this research project.

Thanks are due to several people who added to my understanding of the fundamental details of this research. Dr. Mike Raymer provided insight and understanding for the process of quantum initiation and Dr. Kai Druhl provided theoretical support for our work on soliton initiation.

Finally, I would like to thank Dr. Richard Robiscoe and Dr. Rufus Cone who carefully read this thesis. Their comments are appreciated and have made a definite improvement. This being the last day of National Secretaries Week, I would like to thank the secretaries who have always gone out of their way to be helpful.

TABLE OF CONTENTS

TABLE OF CONTENTS -- Continued

LIST OF TABLES

LIST OF FIGURES

LIST OF FIGURES -- Continued

LIST OF FIGURES -- Continued

ABSTRACT

Theoretical and experimental details of initiating and amplifying a Stokes pulse using stimulated Raman scattering in H_2 are presented. Statistics associated with the spectral fluctuations of a Stokes seed pulse have been measured and theoretically calculated. The spectral fluctuations are shown to result from quantum noise associated with spontaneous initiation. These spectral fluctuations are an example of an easily measurable macroscopic fluctuation of quantum origin. The effects of frequency fluctuations on the generation of solitons in the nonlinear regime of stimulated Raman scattering are calculated and measured.

A detailed derivation of the fully quantum mechanical stimulated Raman scattering equations is given along with their solution for various approximations. The driven Maxwell's equation for the Raman system is derived from the system Hamiltonian. For treating the quantum initiation of stimulated Raman scattering, the radiation field is expanded in localized coherent modes. The details of calculating and using these modes to generate an ensemble of Stokes pulses are presented along with specific examples and ensemble average statistics. The use of localized modes for treating the pulsed cavityless Raman laser gives insight into the spontaneous initiation of Stokes pulses.

A numerical treatment of soliton initiation and formation in stimulated Raman scattering using a π phase shift is given. The π phase shift is produced in the Stokes seed by modulating its envelope through zero. It is found that by modulating the envelope slowly compared to the coherence decay time, T_2, a soliton pulse is initiated which narrows to be much shorter than T_2. Our calculations also confirm the prediction that solitons initiated using an off resonance seed decay during formation.

Solitons have also been observed in the pump and Stokes pulses from a Raman generator. It was predicted that solitons would form in the generator due to random phase shifts caused by quantum initiation. We have confirmed these predictions and measured the amplitude distribution of the spontaneous solitons.

CHAPTER 1

INTRODUCTION

The first documented observation of a solitary wave was made in 1834 by a Scottish scientist and engineer, John Scott Russel[1]. The wave was generated when a canal barge abruptly stopped. From the turbulence a solitary wave formed which propagated one or two miles along the canal before being damped out.

At present there are examples of solitary waves or solitons in several branches of physics[1]. Solitons are localized disturbances which retain their shape as they propagate. Solitons result from a balance between the competition of two effects in a nonlinear system. The above example of water waves results from a competition between dispersion and the nonlinearity which arises when the depth of the water is comparable to the amplitude of the wave. The nonlinear equation governing wave propagation in shallow water is called the Korteweg de Vries (KdV) equation. Other equations which admit soliton solutions are the Modified KdV, sine-Gordon, and Nonlinear Schrodinger (NLS) equation.

The classic example of an optical systems which admits soliton solutions is Self Induced Transparency (SIT)[2]. For this example a coherent optical pulse propagates in a medium of two level atoms. The competition which allows soliton propagation in SIT is between absorption by the medium during the leading part of the pulse and amplification of the pulse by the medium during the trailing part of the pulse. SIT obeys the sine-Gordon equation and the nonlinear equations which govern Stimulated Raman scattering (SRS) can also be transformed into the sine-Gordon equation. Another example of optical soliton propagation in a nonlinear medium occurs in optical fibers[3]. These solitons which are described by the NLS equation result from the balance between dispersion and an amplitude dependent nonlinearity.

The soliton in SRS is the only known example of a three wave soliton. The Raman soliton exists as a localized disturbance in two optical fields and a polarization pulse in the Raman medium. Solitons are initiated in SRS by placing phase shifts in an optical field before it enters the Raman active medium. There are two things about solitons in SRS that are of particular interest. First the solitons are to some degree stable or, in other words, they do not break apart as they propagate. The second interesting feature is that as the soliton propagates it is able to drive atoms from a sparsely populated excited state into the heavily populated ground state. This effect occurs as the later half of a soliton pulse interacts with the medium.

The goal of this research was to obtain an understanding of the fundamental interactions involved with transient Raman scattering. The intention was to investigate the propagation of intense laser pulses and study the effects of phase shifts in a transient medium. Such studies are important to establish a pool of knowledge and techniques which can be of general use in the study of laser beam propagation in a variety of systems.

At the beginning of this research project the primary goal was to study the formation and propagation of solitons in SRS. The solitons had been predicted theoretically[4] and had also been observed experimentally[5]. The first observations were accidental and the origin of the solitons was not understood. Subsequent experiments to initiate Raman solitons using sudden phase shifts did not reliably generate solitons[6]. The primary goal of my research project was to demonstrate that solitons could be reproducibly generated in SRS. In addition we wanted to obtain an understanding of how a phase shift caused a soliton to form. The effects of phase shifts in coherent scattering processes has been virtually unexplored. In the Raman system the phase shift reverses the direction of gain. An understanding of this process may lead to new experiments in other systems.

Our experiments did in fact generate Raman solitons using laser pulses with phase shifts[7]. However, the amplitude of the generated solitons was found to vary greatly for identical experimental conditions. While investigating the cause of the amplitude variations, we discovered that the spectrum of light generated using SRS also had large fluctuations from pulse to pulse[8]. We have now determined that the spectral fluctuations were due to quantum-mechanical noise. Much of this thesis deals with the calculations and measurements of spectral fluctuations. We found that an understanding of these fluctuations was necessary to understand the statistics associated with soliton generation in SRS.

Other systems which have produced macroscopic fluctuations of quantum origin are the cavityless dye laser[9] and superfluorescence[10]. These are both examples of nonoscillating optically pumped lasers. The dye laser uses a grating for one feedback mirror. As in stimulated Raman scattering, the macroscopic fluctuations in the dye laser appear as shot to shot spectral variations. The superfluorescence system consists of a pencil shaped two level medium which is initially completely inverted. Light pulses are emitted from both ends of the medium by the collective emission of all the two level atoms. Macroscopic fluctuations appear in the time delay between inverting the system and detecting the light pulses.

Quantum noise is present to varying degrees in all light. For some cases, such as a single mode laser operating well above threshold, the noise is very small compared to the average signal. On the other hand, thermal sources have noise which is as large as the average intensity. For most cases the variations in thermal light is so rapid that it cannot be resolved. Because quantum noise is always present, it is important to understand and characterize the noise for various sources. Since Raman scattering is an important method of shifting the frequency of a laser to obtain a light source at lower frequency, the spectral fluctuations which we observed will be important for many applications. It is often the case that understanding the light source used in an experiment is an important part of understanding the experiment.

The stimulated Raman scattering system is an example of single pass cavityless laser. Understanding quantum initiation and amplification in such a laser is helpful when trying to form a conceptual picture of how a quantized field interacts with an atomic system. Because there is no cavity, the choice of modes for expanding the field is not obvious. The research that we have done explores selecting a localized set of modes which evolve during amplification.

All lasers are initiated by spontaneous emission. Spontaneous emission results from a quantum mechanical fluctuation. For this reason I will often refer to the spontaneous emission as quantum initiation.

While our experiments were being carried out, it was predicted[11] that in addition to the phase-shift induced Raman solitons, solitons resulting from quantum noise should also be observed. These solitons are a macroscopic signal resulting from quantum noise. We were able to observe these solitons and verify the theoretically predicted[12] amplitude distribution.

The Raman Scattering System

In this section the experimental system used to perform SRS is described. The medium that was used for Raman scattering was H_2 at 10 or 30 atm. The important energy levels are shown in Figure 1. Level (1) is the ground state and level (2) is an electronic excited state. Level (3) is the lowest vibrational excited state. The levels represented by the upper and lower dashed lines are virtual or dressed states. The virtual levels are generated by the fields which oscillate at angular frequencies ω_p and ω_s. The field oscillating at ω_p is the pump laser field which for our experiments was the output from a frequency doubled Neodymium Yttrium Aluminum Garnet (Nd:YAG) laser. The wavelength of this light is 532nm which is green. The field oscillating at ω_s is the Stokes field which grows up from spontaneous Raman emission. The wavelength of the Stokes light is 680nm which is red. When an H_2 molecule is driven by an intense field at ω_p, it will oscillate at ω_p even though there are no nearby levels. This oscillation can be thought of as arising from a superposition of level (1) and the upper virtual level. The virtual level exists to the extent that the molecule oscillates at ω_p. Because the pump field is so far off resonance, it must be very intense in order to produce a significant oscillation at ω_p.

When deriving the equations governing SRS in Chapter 2, I will allow for a possible detuning of the Stokes beam from level (3). This will be important when treating the decay of Raman solitons in Chapter 5. This detuning comes about from quantum fluctuations. Except for the detuning Δ_ϵ, the energy levels in Figure 1 have been drawn to scale.

As shown in the figure there are two possible time orderings for Raman scattering. For the upper path, a molecule absorbs a pump photon and then emits a Stokes photon leaving the molecule in the vibrational state (3). The 1-3 transition is not dipole allowed making the decay of level (3) negligible for time scales which are shorter than or equal to the duration of the pump pulse. For the opposite time ordering, the molecule first emits a Stokes photon and then absorbs a pump photon to again end up in level (3). The coupling strength of the two paths depends on the detuning of the respective virtual level from level (2). The upper virtual level is detuned by Δ_p and the lower virtual level is detuned by $\Delta_p + \omega_p + \omega_s$. Because Δ_p is so large, the lower time ordering cannot be neglected. The inclusion of the lower time ordering does not significantly complicate the

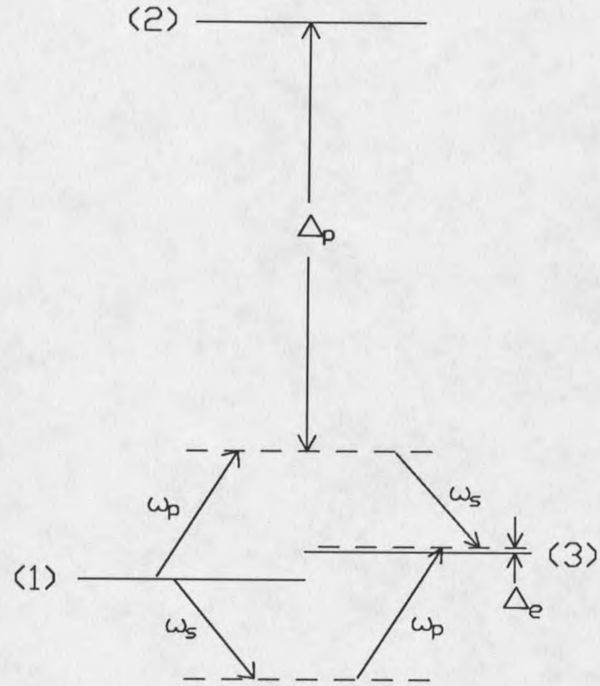

Figure 1 Energy level diagram for stimulated Raman scattering.

mathematical treatment.

There are several important time scales to consider when treating SRS. The slowest time scale is the decay of level (3) to level (1) which is on the order of milliseconds. This is such a long time that it can be considered infinite. The next slowest time scale is the duration of the pump laser pulse which is 20 to 30 nsec. The temporal shape of pulses with this duration are easily measured using a photo-diode and a 400MHz storage oscilloscope. Next on the time scale is the collisional dephasing rate (Γ) which is approximately 1/(0.6nsec) and 1/(0.18nsec) for hydrogen pressures of 10 and 30 atm respectively[13]. The fastest time scale is $1/\Delta_p$ which for our experiments is 0.037fsec.

This is the time required for a molecule to realize that the pump is not on resonance with the 1-2 transition.

The characteristic decay time associated with the collective oscillation of the medium is $1/\Gamma$. The pump and Stokes fields drive the molecules into a superposition of levels (1) and (3), and to a very small extent level (2). The amplitude in level (3) is always much less than 1. The superposition of levels (1) and (3) results in a quadrupole oscillation at $\omega_{31} = \omega_3 - \omega_1$. The phase of this oscillation is determined by the phase of the pump and Stokes field. The collective oscillation of all the atoms gives rise to a macroscopic quadrupole oscillation. When a molecule undergoes a collision, its phase is either partially or completely randomized. When a molecule's phase has been randomized, it no longer contributes to the collective oscillation.

Due to the large detuning Δ_p, the three-level system can effectively be reduced to a two-level system. The amplitude of the virtual states is always small and it comes to equilibrium very quickly allowing the turn-on effects to be neglected for the virtual states. This greatly simplifies the calculations by effectively reducing the system to a two-level problem[14]. The detuning Δ_e can then be thought of as the effective two level detuning. This detuning turns out to be very important for studying soliton generation.

The pump field generates a small amplitude in the virtual states allowing light at the Stokes frequency to be emitted by spontaneous emission. This light will be emitted in all directions and a small portion of it will be emitted in the direction of the pump laser beam. This portion of the spontaneous emission will stimulate further emission at the Stokes frequency. If the length of the medium and the intensity of the pump is large enough, the Stokes pulse will grow until portions of the pump pulse are completely depleted.

To perform SRS, the pump laser beam can simply be focussed into a long cell containing hydrogen. As will be shown, SRS is a nonlinear process requiring high intensities so focussing is usually needed. For gaussian-like temporal pulses, the very front and back of the pump will not be depleted due to the lower intensity in those regions. For our experiments roughly 80% of the pump photons were converted into Stokes photons.

To effectively increase the length of the Raman scattering medium, we used Multi Pass Cells[15] (MPC). The MPC refocuses the pump and Stokes beams several times through the hydrogen cell. However, each focus is at a new location in the cell, so the system can be modeled as a single pass cell with many focuses. In addition to increasing the length of the medium, the MPC suppresses parasitic processes such as second Stokes scattering and anti-Stokes scattering because of dephasing in the cell windows.

Quantum Initiation of Stimulated Raman Scattering

In effect, a stimulated Raman scattering system is a single pass laser with several similarities to a laser that amplifies light which oscillates between two mirrors. Although the Raman laser does not use a population inversion in the usual sense, the Stokes pulse is initiated by spontaneous emission and is amplified to saturation similar to the initiation in a cavity laser.

In order to treat the problem of quantum initiation, the field as well as the molecules must be treated quantum mechanically[16]. For most optics problems, the semi-classical treatment, for which the medium is treated quantum mechanically and the field classically, is sufficient. In order to treat the field quantum mechanically, we must choose a set of radiation modes for describing the field. Once the modes have been chosen, quantum mechanics will tell us the probability distribution for the number of photons in each of the modes. In general, the number of photons in one mode will not be independent from the number in another mode.

In order to treat a single pass Raman laser, Raymer et al.[17] adapted a choice of modes based on the correlation function of the generated Stokes pulses. The resulting set of modes is referred to as the coherent modes. Although generating the coherent modes requires substantial numerical calculations, generating statistics using the coherent modes is simplified. The simplification results from the requirement that the level of excitation of each coherent mode is independent of the other modes. Because the modes are not correlated, ensemble members of the Stokes field can be generated by simply adding the modes together with random phases and statistically weighted amplitudes.

As a result of the quantum mechanical initiation process, macroscopic fluctuations can occur. A mode of the radiation field which grows up from spontaneous emission will be in a chaotic state until it saturates its energy sources.[18] The statistics associated with chaotic states will be given in Chapter 3. The important feature of a mode in a highly excited chaotic state is that the range of possible energies or number of photons in the mode is very broad. This is to say that an ensemble of identically prepared chaotic modes will have a significant fraction of members containing only a few photons as well as members containing large numbers of photons. This broad distribution is the source of macroscopic fluctuations in a variety of experiments. Using the coherent modes description, the statistics of Stokes pulse energies have been predicted[19]. This distribution was also measured[20] and good agreement was obtained. Our experiments involved measuring the spectral fluctuations in the Stokes pulses. Spectral fluctuations arise when more than one mode is excited into a chaotic state. A simple example of this effect is a pulsed laser which is allowed to oscillate in a few longitudinal modes. If the laser is operated below saturation each mode will be in a chaotic state. If the laser cavity has a high quality factor each mode of the laser will appear as a narrow peak in the laser spectrum. Since the energy in each mode is highly uncertain, the relative amplitudes of the peaks in the spectrum will be quite different from shot to shot[21]. This is an example of macroscopic fluctuations which arise from the spontaneous emission.

More dramatic spectral fluctuations can be produced if the quality factor of the above described laser is decreased. This will increase the width of the spectral peaks for each cavity mode. In fact, the width can become larger than the spacing between adjacent modes. For this situation, the spectrum will have more dramatic fluctuations because the spectral peaks from various modes will interfere with each other in a random way. Since the phase of each mode is random, on some shots two adjacent modes can interfere constructively and on others destructively.

For a single pass laser, such as the Raman laser, there is no cavity to choose the modes. To treat the problem we want to use the choice of modes which makes the calculations simplest. For the coherent modes choice, the spectrum of each mode is centered at the same frequency resulting in significant overlap of many modes. This large spectral overlap give rise to large fluctuations.

We used the coherent modes theory to treat the spectral fluctuations in SRS and good agreement with experiment was obtained[22]. The details of this calculation are given in Chapter 3. Our calculations generate ensemble members of output Stokes pulses which are used to generate statistics.

In order to treat quantum fluctuations, we must know how to treat the spontaneous emission process. There are two distinct ways to interpret spontaneous emission[10,23,24]. In one interpretation, vacuum fluctuations stimulate atoms to emit a photon. This interpretation arises when anti-normal ordering of the field operators is used. The other interpretation is called radiation reaction. For this interpretation, molecular polarization fluctuations drive a radiation mode which then couples back to the molecules causing them to emit photons. The coherent modes approach uses polarization fluctuations to initiate the Stokes pulse[17]. We have also applied the vacuum field approach and obtained similar results[22].

To give an intuitive picture of how spectral fluctuations arise from the vacuum field, we need to understand the spectrum of the vacuum field. The vacuum field is considered to be white noise meaning that it has a uniform spectrum. However if one looks at the spectrum of a pulse of white noise it will not be uniform at all. The spectrum will be quite noisy with a characteristic frequency scale which is given by one over the temporal length of the pulse. The average spectrum of several pulses would give the uniform spectrum of white noise.

Our SRS experiment[8,22] with a pulsed pump laser amplifies a temporal segment of white noise. Thus when the spectrum of an individual Stokes pulse is observed, it will have fluctuations on the scale of one over the Stokes pulse length. Since SRS only amplifies a narrow range of frequencies, when the spectrum of many shots are averaged together the result will not be a uniform spectrum but rather an average spectral line shape.

Solitons in Stimulated Raman Scattering

Before describing soliton solutions I will describe what is meant by a general solution to the SRS system. The inputs to a Raman amplifier are arbitrary pump and Stokes fields. Before these pulses arrive, the molecules in the medium are assumed to be in the ground state. Given the temporal envelopes and phases of the input fields, a general solution would tell us the envelopes and phases of the fields at the exit of the Raman amplifier. Because SRS in an amplifier is described by a set of nonlinear differential equations, a general solution does not exist. The soliton solution is a special solution which is valid for a special class of input fields.

To help understand the nonlinear SRS process, it is useful to define three time scale regimes. When the envelopes of the fields vary slowly compared to the collisional dephasing time the system is in the *steady state* regime. The opposite limit where the field envelopes vary much faster than the dephasing time is called the *hypertransient* regime. Intermediate between these situations is the *transient* regime. While our experiments probe all three regimes, the most interesting is the transient regime.

In 1975, Chu and Scott[4] considered a number of nonlinear wave-wave scattering problems using the inverse scattering transform. They found that the SRS equations admitted a soliton solution in the limit that collisional dephasing could be neglected (hypertransient regime). Damping can be neglected for pulses which are much shorter than the damping time. The form of the soliton solution is a hyperbolic secant for the pump field's temporal envelope, a hyperbolic tangent for the Stokes field envelope, and a hyperbolic secant for the oscillation in the medium as a function of time. Because there are three quantities involved, the Raman soliton is referred to as a three wave soliton. Soliton formation with more waves has also been studied[25].

We would like the solution for the fields to go to zero for times before the pulse arrives and after the pulse has passed. The $\tanh(t)$ solution for the Stokes field goes to ± 1 for $t = \pm\infty$. This boundary condition is not a significant problem as long as the Stokes pulse does not go to zero in the region of the soliton. For this case, the soliton solution is valid in the region of the soliton but does not hold in the temporal wings of the pulse.

In 1983, short pulses were observed[5] in a Raman amplifier which was pumped by a CO_2 laser. These pulses were identified as the predicted Raman solitons. Although the original theoretical calculations by Chu and Scott had not predicted how such soliton pulses could be produced, the agreement between experimental data and computer modeling by Druhl[26] using instantaneous π phase shifts in the Stokes seed indicated that the soliton like pulses were being initiated in the transient regime. Once initiated, the pulses narrowed due to damping until they were so short that damping could be neglected. Again one of the important features of the soliton pulses is that they are stable and do not fall apart during the formation process.

The hyperbolic tangent solution for the Stokes pulse crosses through zero at the center of the soliton. This zero crossing gives a π phase shift between the front and the back of the Stokes pulse which led Druhl to use a π phase shift in the input Stokes seed for modeling the soliton formation that was originally observed. The source of the phase shifts in the original experiments were not understood. Subsequent experiments[6] in the Infra-Red (IR) in which a π phase shift was induced in the Stokes seed failed to reproducibly generate soliton pulses. The difficulties in this experiment were attributed to problems with working in the IR. It is difficult to work in the IR because most detectors including the human eyes are not sensitive in this region.

To improve on the previous experiments, we used a visible laser to pump the Raman medium. To initiate a soliton to form in a Raman amplifier, a pump laser pulse and a Stokes seed pulse were combined and injected into the amplifier cell. The Stokes seed was produced in a separate Raman generator. Before entering the amplifier, a π phase shift was produced in the seed pulse by passing it through a crystal whose index of refraction depends on the voltage applied across the crystal. The voltage on the crystal was abruptly changed when the seed pulse was half way through the crystal. This caused the latter half of the pulse to see a greater optical path length than the first half. If the change in path length is half of a wavelength, a π phase shift results between the front and back of the pulse.

As with solitons in other systems such as water waves in a narrow channel and self induced transparency[27], solitons in SRS result from the competition between two effects. The competing effects in the SRS system are forward Raman scattering before the phase shift and inverse Raman scattering after the phase shift. For inverse Raman scattering the pump pulse grows and the Stokes pulse is depleted.

The SRS equations can be transformed into the more familiar sine-Gordon equation.

The sine-Gordon equation also governs self induced transparency in which a single optical field propagates in a medium of two level atoms. Using the sine-Gordon form, Steudel[28] treated the initial pulse resulting from a π phase shift in the Stokes seed. His approximations are valid in the region before significant pump depletion occurs. Meinel[29] used the Backlund transformation to treat the problem of higher order solitons in both SRS and two-photon propagation. However no physical meaning has yet been associated with higher order solitons[30].

Considerable theoretical work has been done on the problem of treating soliton propagation when the damping is small but not small enough to be neglected. Kaup[31] developed a modified inverse scattering transform to include weak damping in the SRS soliton propagation. Druhl and Alsing[32] used a perturbative approach to include weak damping. In Chapter 5, a physical approach to the weak damping problem is presented which uses energy conservation to predict the width of the evolving soliton pulse. Numerical calculations have also been carried out for soliton generation using a Stokes seed which is off resonance[33,34]. This corresponds to a nonzero Δ_ϵ in Figure 1. These calculations show that an off resonance seed causes the soliton pulse to decay during formation. Due to quantum fluctuations, seed pulses from the generator can be off resonance in the amplifier. Correctly predicting the statistics of soliton decay was one of the major goals of my research.

As mentioned earlier one of the properties of a soliton pulse is that it propagates without changing its shape. For any physical system which is governed by a set of nonlinear equations which admit a soliton solution, the nonlinear equations will, to some extent, be an approximation. During the formation of a Raman soliton, the soliton soliton is a poor approximation. Nonetheless, the forming pulse is often referred to as a soliton.

Due to the stability of the SRS soliton, Bowden and Englund[11,35,36] predicted that quantum fluctuations during spontaneous emission in a Raman generator can lead to spontaneous soliton generation. These solitons appear as a macroscopic affect of quantum fluctuations. Experimental observations of spontaneous solitons are presented in Chapter 6.

The thesis is organized in the following manner. In Chapter 2 the equations needed to describe stimulated Raman scattering are derived in detail. The solution to these equations is then given for various approximations. Chapter 3 describes the use of localized modes for theoretically generating ensemble members of Stokes pulses from a Raman generator. Other methods of generating ensemble members are also used. Chapter 4 describes the experiment that we performed to measure statistics associated with quantum noise. A theoretical treatment of soliton generation in SRS is given in Chapter 5 and the soliton experiment is discussed in Chapter 6. Chapter 7 contains a summary of what we have accomplished.

CHAPTER 2

DERIVATION AND SOLUTION OF SRS EQUATIONS

To describe Stimulated Raman Scattering (SRS) before pump depletion, two coupled differential equations are needed. One equation describes how the Stokes pulse evolves from one location in the medium to the next due to an oscillating polarization in the medium. The other equation describes how the medium responds to the driving pump and Stokes fields. The Raman scattering process converts photons from the input pump pulse to photons of lower frequency in the Stokes pulse. If a significant number of photons are taken from the pump pulse, the shape of its temporal envelope will change. If this occurs a third equation is needed to describe how the pump pulse is depleted by the polarization in the medium and the Stokes field.

In this chapter the mathematics for treating the generation of a Stokes pulse from quantum noise and its subsequent amplification is developed. In the first section, the equation of motion for the polarization in the medium is presented. This derivation is outlined by Raymer and Mostowski[16] but the treatment given here fills in a lot of steps and gives a more complete explanation of the approximations used. In the second section the equation governing the growth of the Stokes field is derived from the system Hamiltonian. This derivation was done independently and I have not found a similar derivation in the papers which I have read. Normally Maxwell's equation for the field is used without being derived from the Hamiltonian. In the later sections, solutions to the SRS equations are presented for various approximations.

For the reader who is not interested in the details of how the equations are derived, the operator equations for the Stokes field and polarization in the medium are given in Equations 2.27 and 2.55. The properties of the Langevin noise operator are important for understanding quantum noise so reading should continue in the third section.

A Raman generator can effectively be divided into three regions. In the first region, which is the quantum initiation region, the Stokes field grows from quantum noise to an amplitude which is large enough that the fields can be treated classically. The second region is the linear growth region where the Stokes growth can be modeled by two coupled linear equations and the pump can be assumed to be a prescribed input field. The linear region extends from the quantum initiation region to the location in the medium where the pump intensity has measurable depletion. The third region is the nonlinear growth region. In this region the dynamics of the pump field must be taken into account. This adds a third equation to the system and it becomes nonlinear. A general solution exists for the quantum initiation and linear regions. However, a general solution for the nonlinear region exists only in the steady state approximation[37]. Two coupled equations, one for the medium and one for the Stokes field, are needed when modeling the Stokes evolution in the initiation and linear regions. To theoretically model the system in the nonlinear region, the results obtained by evaluation of the exact solution at the end of the linear region are used as inputs for numerical propagation through the nonlinear region.

The general solution to the linear equations properly accounts for the quantum nature of the Stokes light and the medium but cannot account for pump depletion. The nonlinear set of equations, which must be integrated numerically, are not well suited for treating the quantum initiation but they are appropriate for the linear region as well as the nonlinear region. Both methods are valid in the linear region so there is no problem changing from the quantum solution to the nonlinear equations in the linear region. If the quantum mechanical operators are replaced by c-numbers (classical variables) and appropriate fluctuating noise is used for the initial Stokes field, the nonlinear equations can be used for the entire calculation[11,38].

The equations of motion for the Stokes field and the Raman medium are derived using the Heisenberg equation of motion, taking the full quantum nature of the Stokes field account. The pump field will be treated as a prescribed input classical field which is valid before pump depletion because of the large number of photons in the pump pulse. The hermitian conjugate of an operator which is normally designated by a dagger will be designated by a superscript "+". For some operators, it is necessary to designate the positive or negative frequency components. This is done by including a superscript "(+)" or "(-)" in parenthesis. The Hamiltonian for the system in the Heisenberg picture is[39]

$$\hat{H}(t) = \sum_j \sum_{i=1}^{3} \hbar\omega_i \hat{\sigma}^j_{ii}(t) + \sum_\lambda \hbar\omega_\lambda \hat{a}^+_\lambda(t)\hat{a}_\lambda(t) - \sum_j \hat{\mu}^j(t) \cdot \hat{E}(z^j, t) \tag{2.1}$$

where the $\hat{\sigma}^j_{ij}(t)$ are atomic operators for the jth atom which at $t = 0$ are explicitly written as $\hat{\sigma}_{ij}(0) = |\, i\rangle\langle j\,|$. The annihilation operator, $\hat{a}_\lambda(t)$, is the operator for the radiation mode having angular frequency ω_λ and which is quantized in a volume of length L and area A. Periodic boundary conditions are assumed, and the label λ designates both the wavelength of the mode and its polarization. The sum over λ should be interpreted as a sum over modes having a frequency near the Stokes frequency. The dipole moment operator for the jth atom is $\hat{\mu}^j(t)$. The first term in the Hamiltonian gives the energy associated with the free atoms, and the second term gives the free Stokes field energy. The third term represents the dipole interaction between the atoms and the fields. The dipole operator for the jth atom is[39]

$$\hat{\mu}^j(t) = \vec{\mu}_{12}\hat{\sigma}^j_{12}(t) + \vec{\mu}_{23}\hat{\sigma}^j_{23}(t) + \vec{\mu}^*_{12}\hat{\sigma}^j_{21}(t) + \vec{\mu}^*_{23}\hat{\sigma}^j_{32}(t) \tag{2.2}$$

where $\vec{\mu}_{12}$ and $\vec{\mu}_{23}$ are the dipole matrix elements between levels 1 and 2 and levels 2 and 3 respectively. For example the dipole matrix element between levels 1 and 2 is

$$\vec{\mu}_{12} = e \langle 1|\vec{x}|2\rangle \quad . \tag{2.3}$$

The total field operator, $\hat{\mathrm{E}} = \vec{E}_p + \hat{E}_s$, is the sum of the pump and Stokes fields. The classical pump fields are given by

$$\vec{E}_p(z,t) = \mathrm{E}_p(z,t)\exp[i(\omega_p t - k_p z)]\,\vec{\varepsilon}_p + \mathrm{E}_p^*(z,t)\exp[-i(\omega_p t - k_p z)]\,\vec{\varepsilon}_p \quad . \tag{2.4}$$

The Stokes field is expressed in terms of the slowly varying envelope operators $\hat{\mathrm{E}}_s^{(+)}(z,t)$ and $\hat{\mathrm{E}}_s^{(-)}(z,t)$ using the definition[16]

$$\hat{E}_s(z,t) = \hat{\mathrm{E}}_s^{(-)}(z,t)\exp[i(\omega_s t - k_s z)]\,\vec{\varepsilon}_s + \hat{\mathrm{E}}_s^{(+)}(z,t)\exp[-i(\omega_s t - k_s z)]\,\vec{\varepsilon}_s \tag{2.5}$$

where the (+) and (-) denote the positive and negative frequency components of the field. Note the slight difference in the type used to represent the various field quantities.

$\hat{\mathrm{E}}(z,t)$ is the total field operator.

$\vec{E}_p(z,t)$ is the total pump field.

$\mathrm{E}_p(z,t)$ $(\mathrm{E}_p^*(z,t))$ is the positive (negative) part of the pump field.

$\hat{E}_s(z,t)$ is the total Stokes field operator.

$\hat{\mathrm{E}}_s^{(+)}(z,t)$ $(\hat{\mathrm{E}}_s^{(-)}(z,t))$is the positive (negative) part of the slowly varying Stokes field operator.

$\hat{E}_s^{(+)}(z,t)$ $(\hat{E}_s^{(-)}(z,t))$is the positive (negative) part of the Heisenberg Stokes field operator.

At this point I will not write $\hat{E}_s^{(+)}(z,t)$ and $\hat{E}_s^{(-)}(z,t)$ in terms of creation and annihilation operators because they can in general be different operators than those which appear in the Hamiltonian. The operators that appear in the Hamiltonian are Heisenberg operators and thus contain all of the time dependence of the field. Therefore when the equation of motion for the field operators is calculated using Equation 2.1 the field must be expressed in terms of the cavity mode operators.

Derivation of the Medium Equation

The derivation in this section is similar to that given in reference 16. To obtain the equations of motion for the atomic operators, the equation

$$i\hbar\frac{d\hat{O}}{dt} = [\hat{O}, \hat{H}] \tag{2.6}$$

is used where $\hat{O}$ is an arbitrary operator without explicit time dependence. Using Equation 2.6 and noting that $\hat{\sigma}^j_{im} \times \hat{\sigma}^j_{mk} = \hat{\sigma}^j_{ik}$, the equations of motion for the three atomic superposition operators are calculated to give

$$\frac{d\hat{\sigma}^j_{31}(t)}{dt} = i\omega_{31}\hat{\sigma}^j_{31}(t) + \frac{i}{\hbar}[\vec{\mu}_{12}\hat{\sigma}^j_{32}(t) - \vec{\mu}_{23}\hat{\sigma}^j_{21}(t)] \cdot \hat{E}(z^j,t) \tag{2.7}$$

$$\frac{d\hat{\sigma}^j_{21}(t)}{dt} = i\omega_{21}\hat{\sigma}^j_{21}(t) + \frac{i}{\hbar}\left[\vec{\mu}_{12}(\hat{\sigma}^j_{22}(t) - \hat{\sigma}^j_{11}(t)) - \vec{\mu}^{\,*}_{23}\hat{\sigma}^j_{31}(t)\right] \cdot \hat{\mathrm{E}}(z^j, t) \tag{2.8}$$

$$\frac{d\hat{\sigma}^j_{32}(t)}{dt} = -i\omega_{23}\hat{\sigma}^j_{32}(t) + \frac{i}{\hbar}\left[\vec{\mu}_{23}(\hat{\sigma}^j_{33}(t) - \hat{\sigma}^j_{22}(t)) + \vec{\mu}^{\,*}_{12}\hat{\sigma}^j_{31}(t)\right] \cdot \hat{\mathrm{E}}(z^j, t) \tag{2.9}$$

where $\omega_{ij} = \omega_i - \omega_j$ and the commutator, $[a, \sigma_{ij}] = 0$ has been used. It will be shown in the later part of this section that the Stokes field operator will be driven by $\hat{\sigma}_{13}$. To this end, Equations 2.8 and 2.9 are formally integrated and the results substituted into Equation 2.7. It is interesting to note that equations of motion for the diagonal operators are not needed partially because the assumption that $\langle\hat{\sigma}_{11}\rangle = 1$ (which is valid even for complete pump depletion) will eventually be made and partially because of the effective elimination of level 2. The results of integrating Equations 2.8 and 2.9 are

$$\hat{\sigma}^j_{21}(t) = \hat{\sigma}^j_{21}(0)\exp(i\omega_{21}t) + \frac{i}{\hbar}\int_0^t \exp[i\omega_{21}(t-t')]$$
$$\left\{\vec{\mu}_{12}[\hat{\sigma}^j_{22}(t') - \hat{\sigma}^j_{11}(t')] - \vec{\mu}^{\,*}_{23}\hat{\sigma}^j_{31}(t')\right\} \cdot \hat{\mathrm{E}}(z^j, t')dt' \tag{2.10}$$

$$\hat{\sigma}^j_{32}(t) = \hat{\sigma}^j_{32}(0)\exp(-i\omega_{23}t) + \frac{i}{\hbar}\int_0^t \exp[-i\omega_{23}(t-t')]$$
$$\left\{\vec{\mu}_{23}[\hat{\sigma}^j_{33}(t') - \hat{\sigma}^j_{22}(t')] + \vec{\mu}^{\,*}_{12}\hat{\sigma}^j_{31}(t')\right\} \cdot \hat{\mathrm{E}}(z^j, t')dt' \quad . \tag{2.11}$$

The initial conditions are that the system starts in the ground state and the initial atomic operators are $\hat{\sigma}^j_{21}(0) = |2\rangle\langle 1|$ and $\hat{\sigma}^j_{32}(0) = |3\rangle\langle 2|$. When the integrals in Equations 2.10 and 2.11 are performed and the results are substituted into Equation 2.7, only the terms that oscillate near ω_{31} need to be kept. The terms in the integrals containing $\hat{\sigma}^j_{31}$ have parts which oscillate at the frequency needed to drive the pump-Stokes transition. These terms arise from combinations of $\mathrm{E}_p(z^j,t)$ and $\mathrm{E}^*_p(z^j,t')$ and also from combinations of $\hat{\mathrm{E}}^{(-)}_s(z^j,t)$ and $\mathrm{E}^{(+)}_s(z^j,t')$ plus terms with the opposite time ordering. However these terms only lead to a Stark shift and thus they can be discarded for this part of the calculation. To see that they will lead to a Stark shift, note that each of these terms will generate a contribution that is proportional to the operator $i\hat{\sigma}^j_{31}(t)$ and thus could be accounted for by simply modifying ω_{31}. The only remaining way to produce an oscillation at ω_{31} is with a combination of $\mathrm{E}_p(z,t) \times \hat{\mathrm{E}}^{(+)}_s(z,t')$ or $\mathrm{E}(z,t') \times \hat{\mathrm{E}}^{(+)}(z,t)$ corresponding to the two possible time orderings shown in Figure 1. Therefore, only these parts of the field will be kept when calculating $\hat{\sigma}_{21}$ and $\hat{\sigma}_{32}$. Rewriting Equation 2.10 and keeping only the terms which can drive the pump-Stokes transition, we obtain

$$\hat{\sigma}^j_{21}(t) = \frac{i}{\hbar}\int_0^t \exp[i\omega_{21}(t-t')] \quad [\hat{\sigma}^j_{22}(t') - \hat{\sigma}^j_{11}(t')] \quad \{\mathrm{E}_p(z^j,t')\exp[i(\omega_p t' - k_p z)] \quad \vec{\mu}_{12}\cdot\vec{\varepsilon}_p$$
$$+\hat{\mathrm{E}}^{(+)}_s(z^j,t')\exp[-i(\omega_s t' - k_s z)] \quad \vec{\mu}_{12}\cdot\vec{\varepsilon}_s\}\,dt' \quad . \qquad (2.12)$$

To carry out the integrals in Equation 2.12, the Slowly Varying Envelope Approximation (SVEA) is used. The SVEA assumes that the envelopes of the fields vary much slower than the individual oscillation of the field. This is a very good approximation because the envelopes typically vary over nanoseconds and the oscillation times are typically femtoseconds. The SVEA is not enough justification by itself for simply pulling the field envelopes and the atomic operators out of the integral. The meaning of the lower limit of the integral must first be understood. The lower limit tells us something about the initial conditions of the system. In the real atom there is damping which would wash out any information about the initial conditions. However, the damping is not very important either because the amplitude of the oscillation of the atom at the driving frequency reaches semiequilibrium on a time scale of a few oscillations. This is because the fields are so far off resonance. The lower limit only determines the point about which $\hat{\sigma}^j_{21}$ oscillates. The time dependence of the slowly varying quantities in the integral and the damping can slightly change the point about which $\hat{\sigma}^j_{21}$ oscillates; however, only the oscillating part will drive $\hat{\sigma}^j_{31}$. Damping will be important in the equation of motion for the operator $\hat{\sigma}_{31}$ because its magnitude will be limited by damping whereas the magnitude of $\hat{\sigma}_{21}$ is limited by detuning. A mathematical justification of the SVEA is given in Appendix A. Making the SVEA and evaluating the integral in Equation 2.12 at the upper limit results in

$$\hat{\sigma}^j_{21}(t) = -\frac{1}{\hbar}(\hat{\sigma}^j_{22}(t) - \hat{\sigma}^j_{11}(t))\left\{\frac{\exp[i(\omega_p t - k_p z)]}{(\omega_{21} - \omega_p)}\mathrm{E}_p \quad \vec{\mu}_{12} \cdot \vec{\varepsilon}_p \right.$$

$$\left. + \frac{\exp[-i(\omega_s t - k_s z)]}{(\omega_{21} + \omega_s)}\hat{\mathrm{E}}^{(+)}_s \quad \vec{\mu}_{12} \cdot \vec{\varepsilon}_s \right\} \quad . \tag{2.13}$$

And, similarly for $\hat{\sigma}^j_{32}(t)$, Equation 2.11 becomes

$$\hat{\sigma}^j_{32}(t) = \frac{1}{\hbar}(\hat{\sigma}_{33}(t)^j - \hat{\sigma}_{22}(t)^j)\left\{\frac{\exp[i(\omega_p t - k_p z)]}{(\omega_{23} + \omega_p)}\mathrm{E}_p(z^j, t) \quad \vec{\mu}_{23} \cdot \varepsilon_p \right.$$

$$\left. + \frac{\exp[-i(\omega_s t - k_s z)]}{(\omega_{23} - \omega_s)}\hat{\mathrm{E}}^{(+)}_s(z^j, t) \quad \vec{\mu}_{23} \cdot \vec{\varepsilon}_s \right\} \quad . \tag{2.14}$$

Next the rapid time dependence in Equation 2.7 is factored out by changing to the slowly varying polarization operator defined by

$$\hat{Q}^j(t) = \hat{\sigma}^j_{31}(t)\exp[-i(\omega_p - \omega_s)t + i(k_p - k_s)z^j] \quad . \tag{2.15}$$

Defining the effective detuning by

$$\Delta_e = \omega_p - \omega_s - \omega_{31} \tag{2.16}$$

and using Equation 2.7, the equation of motion for the slowly varying polarization operator becomes

$$\frac{d\hat{Q}^j(t)}{dt} = -i\hat{Q}^j(t)\Delta_e + \mathrm{I}_1 + \mathrm{I}_2 \tag{2.17}$$

where the two interaction terms are defined by

$$\mathrm{I}_1 = -\frac{i}{\hbar}\exp[-i(\omega_p - \omega_s)t + i(k_p - k_s)z^j] \quad \hat{\sigma}^j_{21}(t) \quad \vec{\mu}_{23} \cdot \hat{\mathrm{E}}(z^j, t) \tag{2.18}$$

$$\mathrm{I}_2 = \frac{i}{\hbar}\exp[-i(\omega_p - \omega_s)t + i(k_p - k_s)z^j] \quad \hat{\sigma}^j_{32}(t) \quad \vec{\mu}_{12} \cdot \hat{\mathrm{E}}(z^j, t) \quad . \tag{2.19}$$

Only the portion of the field in each interaction term, for which the rapid time dependence cancels, needs to be kept. Therefore, only combinations which result in $E_p(z,t) \times \hat{E}_s^{(+)}(z,t)$ are retained. Substituting Equations 2.13 and 2.14 into Equations 2.18 and 2.19, the interaction terms become

$$I_1 = \frac{i}{\hbar^2}[\hat{\sigma}_{22}^j(t) - \sigma_{11}^j(t)]\, E_p(z^j,t)\hat{E}_s^{(+)}(z^j,t)\left\{\frac{(\vec{\mu}_{12}\cdot\vec{\varepsilon}_p)\quad(\vec{\mu}_{23}\cdot\vec{\varepsilon}_s)}{(\omega_{21}-\omega_p)} + \frac{(\vec{\mu}_{12}\cdot\vec{\varepsilon}_s)\quad(\vec{\mu}_{23}\cdot\vec{\varepsilon}_p)}{(\omega_{21}+\omega_s)}\right\} \tag{2.20}$$

and

$$I_2 = \frac{i}{\hbar^2}[\hat{\sigma}_{33}^j(t) - \hat{\sigma}_{22}^j(t)]\, E_p(z^j,t)\hat{E}_s^{(+)}(z^j,t)\left\{\frac{(\vec{\mu}_{23}\cdot\vec{\varepsilon}_s)\quad(\vec{\mu}_{12}\cdot\vec{\varepsilon}_p)}{(\omega_{23}-\omega_s)} + \frac{(\vec{\mu}_{23}\cdot\vec{\varepsilon}_p)\quad(\vec{\mu}_{12}\cdot\vec{\varepsilon}_s)}{(\omega_{23}+\omega_p)}\right\} \tag{2.21}$$

Because the Raman detuning is very much smaller than all other frequencies, the bracketed portions of Equations 2.20 and 2.21 are essentially equal. This can be seen by noting that

$$\Delta_p = \omega_{21} - \omega_p \approx \omega_{23} - \omega_s \quad \text{and} \quad \omega_{21} + \omega_s \approx \omega_{23} + \omega_p \tag{2.22}$$

where Δ_p is the detuning of the pump frequency from ω_{21}. Defining the coupling constant which tells how effective the pump and Stokes fields are at driving the polarization $\hat{Q}^j(t)$ by

$$\kappa_1 = \frac{1}{\hbar^2}\left\{\frac{(\vec{\mu}_{23}\cdot\vec{\varepsilon}_s)\quad(\vec{\mu}_{12}\cdot\vec{\varepsilon}_p)}{\Delta_p} + \frac{(\vec{\mu}_{23}\cdot\vec{\varepsilon}_p)\quad(\vec{\mu}_{12}\cdot\vec{\varepsilon}_s)}{(\omega_{21}+\omega_s)}\right\}\quad , \tag{2.23}$$

we arrive at solution for the jth atom.

$$\frac{d\hat{Q}^j(t)}{dt} = -i\hat{Q}^j(t)\,\Delta_e + i\kappa_1[\hat{\sigma}^j_{33}(t) - \hat{\sigma}^j_{11}(t)] \quad E_p(z^j,t)\hat{E}_s^{(+)}(z^j,t) \quad . \tag{2.24}$$

The above equation can be simplified by assuming that only a small fraction of the atoms are excited into state 3. With this assumption, the combination of diagonal operators is replaced with the unit operator. Calculations performed without this assumption show that on the order of one in a thousand atoms are excited to state 3. To obtain the polarization for the continuous medium, the medium is divided into slices with a thickness much smaller than the wavelength of the fields but thick enough to contain many atoms. The location of each slice is labeled by z and the number of atoms in the slice z is $N_s = N\,A\,\Delta z$ where N is the number density of atoms and Δz is the thickness of the slice. The average polarization in a slice is defined by

$$\hat{Q}(z,t) = \frac{1}{N_s}\sum_{\{j\}_z}\hat{Q}^j(t) \quad . \tag{2.25}$$

Summing Equation 2.24 over all atoms in a slice, or more specifically, summing over the set $\{j\}_z$ and using the fact that $\hat{Q}^j(t), E_p(z^j,t)$, and $\hat{E}_s(z^j,t)$ are nearly identical for all atoms in the slice, Equation 2.24 becomes

$$\frac{d\hat{Q}(z,t)}{dt} = -i\hat{Q}(z,t)\,\Delta_e - i\kappa_1 E_p(z,t)\hat{E}_s^{(+)}(z,t) \quad . \tag{2.26}$$

At this stage, the average operators are used so the average damping can be phenomenologically included. When damping is added, a Langevin noise operator must be added[16]

$$\frac{d\hat{Q}(z,t)}{dt} = -\hat{Q}(z,t)\,(i\Delta_e + \Gamma) - i\kappa_1 \mathrm{E}_p(z,t)\hat{\mathrm{E}}_s^{(+)}(z,t) + \hat{F}(z,t) \quad . \tag{2.27}$$

The properties of the Langevin operator, $\hat{F}(z,t)$, will be discused later in this chapter.

Derivation of the Stokes Field Equation

To obtain the differential equation for the Stokes field, one normally uses Maxwell's equations. In this section, the slowly varying wave equation for the Stokes will be derived using the Hamiltonian and Heisenberg's equation cf. Equation 2.1 and 2.6. This derivation has been done independently from previous work. Since the Hamiltonian is expressed in terms of field operators for radiation modes which are quantized in a cavity, the Stokes field is most conveniently expressed in term of the same modes. In terms of positive and negative frequency components, the Stokes field operator is

$$\hat{E}_s(z,t) = \hat{E}_s^{(-)}(z,t) + \hat{E}_s^{(+)}(z,t) \tag{2.28}$$

where

$$\hat{E}_s^{(-)}(z,t) = -i\vec{e}_s \sum_{\lambda} \hat{a}_\lambda^{\dagger}(t)\, \exp(-ik_\lambda z) = \hat{\mathrm{E}}_s^{(-)}(z,t)\, \vec{\varepsilon}_s\, \exp[i(\omega_s t - k_s z)] \tag{2.29}$$

$$\hat{E}_s^{(+)}(z,t) = i\vec{e}_s \sum_{\lambda} \hat{a}_\lambda(t)\, \exp(ik_\lambda z) = \hat{\mathrm{E}}_s^{(+)}(z,t)\, \vec{\varepsilon}_s\, \exp[-i(\omega_s t - k_s z)] \tag{2.30}$$

and where the polarization vector $\vec{e}_s$ is defined by

$$\vec{e}_s = (\pi\hbar c\, k_s/\mathrm{LA})^{1/2}\, \vec{\varepsilon}_s \equiv \beta^{1/2} \vec{\varepsilon}_s \tag{2.31}$$

and ω_s is the central Stokes frequency. The wave number k_s is assumed to be the same for all modes near the Stokes frequency. Note that all of the time dependence is in the operators $\hat{a}(t)$ and $\hat{a}^{+}(t)$ making them Heisenberg operators. To calculate $\hat{E}_s^{(+)}(z,t)$, the equation for $\hat{a}_\lambda(t)$ will first be derived and then summed over λ. The Heisenberg equation of motion for the operator $\hat{a}_\lambda(t)$ is

$$i\hbar \frac{d\hat{a}_\lambda(t)}{dt} = \hbar \sum_{\lambda'} \omega_{\lambda'} [\hat{a}_\lambda(t)\,, \hat{a}^{+}_{\lambda'}(t)\, \hat{a}_{\lambda'}(t)] - \sum_j\, [\hat{a}_\lambda(t), \hat{\mu}^j(t) \cdot \hat{\mathrm{E}}(z^j, t)] \quad . \tag{2.32}$$

Using the commutation relations

$$[\hat{a}_\lambda(t), \hat{a}^{+}_{\lambda'}(t)] = \delta_{\lambda\lambda'} \quad , \quad [\hat{a}_\lambda(t), \hat{a}_{\lambda'}(t)] = 0 \quad \text{and} \quad [\hat{a}_\lambda(t), \hat{\sigma}_{ij}(t)] = 0 \tag{2.33}$$

it can be seen that only the $\hat{E}_s^{(-)}(z,t)$ part of the total field operator contributes to the interaction term. Formally integrating Equation 2.32 and using Equation 2.29, the equation for the field operator becomes

$$\hat{a}_\lambda(t) = \hat{a}_\lambda(0) \exp(-i\omega_\lambda t) + \frac{1}{\hbar} \sum_j \exp(-ik_\lambda z^j) \int_o^t \exp[-i\omega_\lambda (t - t')] \quad \hat{\mu}^j(t') \cdot \vec{e}_s \quad dt' \quad . \tag{2.34}$$

The operator $\hat{E}_s^{(+)}(z,t)$ is formed by multiplying by $i\vec{e}_s \exp(ik_\lambda z)$ and summing over λ

which gives

$$\hat{E}_s^{(+)}(z,t) = i \sum_\lambda \vec{e}_s\, \hat{a}_\lambda(0) \exp[-i(\omega_\lambda t - k_\lambda z)]$$

$$+ \quad \frac{i}{\hbar}\vec{e}_s \sum_j \sum_\lambda \exp[ik_\lambda(z - z^j)] \int_0^t \exp[-i\omega_\lambda(t-t')] \quad \hat{\mu}^j(t') \cdot \vec{e}_s\, dt' \quad . \qquad (2.35)$$

Now that the equation of motion has been obtained, it is convenient to convert back to the slowly varying operators. Keeping only the oscillation near the Stokes frequency, the slowly varying operators for $\hat{\mu}^j(t)$ are defined by

$$\hat{\mu}_s^j(t) = \hat{\mu}^{j(-)}(t) \exp[i(\omega_s t - k_s z^j)] + \hat{\mu}^{j(+)}(t) \exp[-i(\omega_s t - k_s z^j)] \qquad (2.36)$$

where ω_s is the central Stokes frequency. Keeping the appropriate part of the dipole operator, the slowly varying positive frequency field operator becomes

$$\hat{\mathrm{E}}_s^{(+)}(z,t) = \sum_\lambda i\hat{a}_\lambda(0)\, \beta^{1/2} \exp[-i(\omega_\lambda - \omega_s)t + i(k_\lambda - k_s)z] + \frac{i}{\hbar}\beta^{1/2} \sum_j$$

$$\times \int_0^t \exp[i\omega_s(t-t') - ik_s(z - z^j)] \sum_\lambda \exp[-i\omega_\lambda(t-t') + ik_\lambda(z - z^j)]\ \hat{\mu}^{j(+)}(t') \cdot \vec{e}_s\, dt' \qquad (2.37)$$

where only the positive frequency part of $\hat{\mu}^j(t)$ has been kept because of the Rotating Wave Approximation (RWA). The sum over j can be converted to a sum over slices using

$$\sum_j \Rightarrow \sum_{z'} \sum_{\{j\}_{z'}} \qquad (2.38)$$

and the slice average positive frequency dipole operator is defined by

$$\hat{\mu}^{(+)}(z',t) = \frac{1}{N_s} \sum_{\{j\}_{z'}} \hat{\mu}^{j(+)}(t) \quad . \tag{2.39}$$

Noting that $\omega = kc$, the equation for $\hat{E}_s^{(+)}(z,t)$ becomes

$$\begin{aligned} \hat{E}_s^{(+)}(z,t) = {} & \sum_{\lambda} i\hat{a}_{\lambda}(0)\, \beta^{1/2} \exp[-i(\omega_{\lambda} - \omega_s)t + i(k_{\lambda} - k_s)z] \\ & + \frac{iN_s\beta^{1/2}}{\hbar} \sum_{z'} \int_0^t \exp\{ik_s[c(t-t') - (z-z')]\} \quad \hat{\mu}^{(+)}(z',t') \cdot \vec{e}_s \\ & \times \sum_{\lambda} \exp\{-ik_{\lambda}[c(t-t') - (z-z')]\}\, dt' \quad . \end{aligned} \tag{2.40}$$

The sum over λ can be converted to an integral by letting the quantization length become longer than the pump pulse and then using

$$\sum_{\lambda} \Rightarrow \frac{L}{\pi} \int_{-\infty}^{\infty} dk \sum_{\varepsilon_s} \quad . \tag{2.41}$$

The integral over k will produce a delta function which is explicitly

$$\frac{L}{\pi} \int_{-\infty}^{\infty} dk \exp\{-ik[c(t-t') - (z-z')]\} = \frac{2L}{c} \quad \delta[(t-t') - (z-z')/c] \quad . \tag{2.42}$$

To get a contribution from the delta function when preforming the integral over t', the argument of the delta function must go through zero for t' between zero and t. To satisfy this condition, the limits on the sum over z' are

$$z - ct < z' < z \quad . \tag{2.43}$$

Letting the variable z' become continuous and replacing the sum over z' using

$$N_s \sum_{z'} \Rightarrow \rho \int_{z-ct}^{z} dz' \tag{2.44}$$

where ρ is the linear number density of atoms, the equation for $\hat{E}_s^{(+)}(z,t)$ becomes

$$\hat{E}_s^{(+)}(z,t) = \sum_{\lambda} i\hat{a}_{\lambda}(0)\, \beta^{1/2} \exp[-i(\omega_{\lambda} - \omega_s)t + i(k_{\lambda} - k_s)z] + \frac{i\rho 2L\beta^{1/2}}{\hbar c} \sum_{\varepsilon_s} \int_{z-ct}^{z} \hat{\mu}^{(+)}[z', t - (z - z')/c] \cdot \vec{e}_s dz' \tag{2.45}$$

where $t' \Rightarrow t - (z - z')/c$ as required by the delta function. Now that the equation for $\hat{E}_s^{(+)}(z,t)$ has been found the slowly varying wave equation can be formed using

$$\left[\frac{\partial}{\partial z} + \frac{1}{c}\frac{\partial}{\partial t}\right] \hat{E}_s^{(+)}(z,t) = driving\, term \quad . \tag{2.46}$$

To calculate the necessary derivatives, the following formula is helpful[40]

$$\frac{\partial}{\partial\alpha}\int_{x=f(\alpha)}^{x=g(\alpha)} F(\alpha,x)dx = \int_{x=f(\alpha)}^{x=g(\alpha)} \frac{\partial F(\alpha,x)}{\partial\alpha}dx$$

$$+ \left\{\frac{\partial g(\alpha)}{\partial\alpha}F[\alpha,g(\alpha)] - \frac{\partial f(\alpha)}{\partial\alpha}F[\alpha,f(\alpha)]\right\} \quad . \qquad (2.47)$$

Using this formula, the z derivative of the field operator is

$$\frac{\partial \hat{\mathrm{E}}_s^{(+)}(z,t)}{\partial z} = \sum_\lambda i\hat{a}_\lambda(0)\,\beta^{1/2}\,[i(k_\lambda - k_s)]\exp[-i(\omega_\lambda - \omega_s)t + i(k_\lambda - k_s)z] + \frac{i2\mathrm{L}\rho\beta^{1/2}}{\hbar c} \times$$

$$\sum_{\varepsilon_s}\left\{\hat{\mu}^{(+)}(z,t)\cdot\vec{e}_s - \hat{\mu}^{(+)}(z-ct,0)\cdot\vec{e}_s + \int_{z-ct}^{z} \left.\frac{d\hat{\mu}^{(+)}(z',u)}{du}\right|_{u=t-(z-z')/c}\left(\frac{-1}{c}\right)\cdot\vec{e}_s\,dz'\right\} \qquad (2.48)$$

and the time derivative multiplied by $1/c$ is

$$\frac{1}{c}\frac{\partial \hat{\mathrm{E}}_s^{(+)}(z,t)}{\partial t} = \sum_\lambda i\hat{a}_\lambda(0)\,\beta^{1/2}\,\frac{[-i(\omega_\lambda - \omega_s)]}{c}\exp[-i(\omega_\lambda - \omega_s)t + i(k_\lambda - k_s)z] \quad +$$

$$\frac{i2\mathrm{L}\rho\beta^{1/2}}{\hbar c^2}\sum_{\varepsilon_s}\left\{-\hat{\mu}^{(+)}(z-ct,0)(-c)\cdot\vec{e}_s \quad + \int_{z-ct}^{z}\left.\frac{d\hat{\mu}^{(+)}(z',u)}{du}\right|_{u=t-(z-z')/c}\cdot\vec{e}_s dz'\right\} \quad . \qquad (2.49)$$

Note that the free propagation terms exactly cancel which is what one would expect because free fields propagate without change. The terms containing $\hat{\mu}^{(+)}(z-ct,0)$ cancel and very conveniently the terms containing the integrals also cancel. Adding Equation 2.48 to 2.49, the slowly varying wave equation becomes

$$\left[\frac{\partial}{\partial z}+\frac{1}{c}\frac{\partial}{\partial t}\right]\hat{E}_s^{(+)}(z,t)=\frac{i2L\rho\beta}{\hbar c}\sum_{\varepsilon_s}\hat{\mu}^{(+)}(z,t)\cdot\vec{\varepsilon}_s \quad . \tag{2.50}$$

The second factor of $\beta^{1/2}$ comes from changing $\vec{e}_s$ to $\vec{\varepsilon}_s$.

To evaluate the driving term, we need to keep the part of Equation 2.2 which oscillates as $\exp(-i\omega_s t)$. The parts of the dipole operator which oscillate at the proper frequency can be determined by examining Equations 2.10 and 2.11. First note that the terms in the integrals in Equations 2.10 and 2.11 containing $\hat{\sigma}_{11}(t')$, $\hat{\sigma}_{22}(t')$, and $\hat{\sigma}_{33}(t')$ can be combined with $\hat{E}_s^{(+)}(z^j,t')$ to produce an oscillation at ω_s. However, because these terms are proportional to $i\hat{E}_s^{(+)}(z^j,t')$ it will only lead to change in the index of refraction and can be accounted for by simply changing c to v. For hydrogen gas at the pressures that were used in our experiments, the index of refraction is nearly unity, so the approximation $v = c$ will be used.

It can be seen from Equation 2.7 that $\hat{\sigma}_{31}(t)$ oscillates approximately as $\exp(i\omega_{31}t)$. Combining $\hat{\sigma}_{31}(t')$ with the part of the pump which oscillates as $\exp(-i\omega_p t')$, an oscillation near $\exp(-i\omega_s t')$ will be produced. This is the only combination which contributes to the dipole operator at the correct oscillation frequency. Substituting the $\hat{\sigma}_{31}^j(t')$ terms from Equations 2.10 and 2.11 into Equation 2.2, the positive frequency part of $\hat{\mu}^j(t)$ which oscillates at the appropriate frequency becomes

$$\begin{aligned}\hat{\mu}_s^j(t)=\frac{i}{\hbar}\Bigg\{&-\left(\vec{\mu}_{23}^{\,*}\cdot\vec{\varepsilon}_p\right)\vec{\mu}_{12}^{\,*}\int_0^t \exp[i\omega_{21}(t-t')]\;\hat{\sigma}_{31}^j(t')E_p^*(z^j,t')\exp[-i(\omega_p t'-k_p z^j)]\;dt'\\&+\left(\vec{\mu}_{12}^{\,*}\cdot\vec{\varepsilon}_p\right)\vec{\mu}_{23}^{\,*}\int_0^t \exp[-i\omega_{23}(t-t')]\;\hat{\sigma}_{31}^j(t')E_p^*(z^j,t)\exp[-i(\omega_p t'-k_p z^j)]\;dt'\Bigg\}\quad .\end{aligned} \tag{2.51}$$

Using Equations 2.15 and 2.36, the above equation is converted to the slowly varying operator equation

$$\hat{\mu}^{j(+)}(t) = \frac{i}{\hbar}\left\{-\left(\vec{\mu}_{23}^{\,*}\cdot\vec{\varepsilon}_p\right)\vec{\mu}_{12}^{\,*}\exp[i(\omega_s+\omega_{21})t]\int_0^t \hat{Q}^j(t')\mathrm{E}_p^*(z^j,t')\exp[-i(\omega_s+\omega_{21})t']dt'\right.$$
$$\left. + \left(\vec{\mu}_{12}^{\,*}\cdot\vec{\varepsilon}_p\right)\vec{\mu}_{23}^{\,*}\exp[i(\omega_s-\omega_{23})t]\int_0^t \hat{Q}^j(t')\mathrm{E}_p^*(z^j,t')\exp[-i(\omega_s-\omega_{23})t']dt'\right\} \quad . \qquad (2.52)$$

Using the SVEA approximation, the slowly varying quantities are pulled out of the integral and it is evaluated at the upper limit. Taking the dot product with $\vec{\varepsilon}_s$ and using $\omega_{23}-\omega_s=\Delta_p$, Equation 2.52 becomes

$$\hat{\mu}^{j(+)}(t)\cdot\vec{\varepsilon}_s = \frac{1}{\hbar}\hat{Q}^j(t)\mathrm{E}_p^*(z^j,t)\left\{\frac{\left(\vec{\mu}_{23}^{\,*}\cdot\vec{\varepsilon}_p\right)\left(\vec{\mu}_{12}^{\,*}\cdot\vec{\varepsilon}_s\right)}{(\omega_s+\omega_{21})} + \frac{\left(\vec{\mu}_{23}^{\,*}\cdot\vec{\varepsilon}_s\right)\left(\vec{\mu}_{12}^{\,*}\cdot\vec{\varepsilon}_p\right)}{\Delta_p}\right\} \quad . \qquad (2.53)$$

Converting to slice average operators by summing over the atoms in a slice and dividing by the number of atoms, the positive frequency part of the polarization becomes

$$\hat{\mu}^{(+)}(z,t)\cdot\vec{\varepsilon}_s = \hbar\kappa_1^*\hat{Q}(z,t)\mathrm{E}_p^*(z,t) \quad . \qquad (2.54)$$

The constant κ_1 is defined in Equation 2.23. Substituting the positive frequency polarization operator into Equation 2.50, the driven slowly varying wave equation is obtained

$$\left[\frac{\partial}{\partial z}+\frac{1}{c}\frac{\partial}{\partial t}\right]\hat{\mathrm{E}}_s^{(+)}(z,t) = i\kappa_2\hat{Q}(z,t)\mathrm{E}_p^*(z,t) \quad . \qquad (2.55)$$

The coupling constant κ_2 is defined by

$$\kappa_2 = 2\pi N k_s \hbar \kappa_1^* \quad . \tag{2.56}$$

The sum over ε_s has been omitted by assuming that $\vec{\mu}_{23}$ is parallel to $\vec{\mu}_{12}$.

This concludes the derivation of the fully quantum mechanical SRS equations. Before discussing their general solution, the properties of the Langevin noise operator must be determined. Also, the equations will become simpler when they are transformed to the retarded time frame. The inputs to the equations are the pump and Stokes fields for all times at the entrance to the Raman cell, and the initial polarization of the medium. When this information is specified, the SRS equations will determine the Stokes field for all time at the exit of the cell provided that pump depletion has not occurred.

Properties of the Langevin Noise Operator

In Equation 2.27, a Langevin noise operator was included to maintain the operator properties of $\hat{Q}(z,t)$. The properties of the Langevin operator can be found by adding a random kick term in the Hamiltonian[41]. The kicks are assumed to be short compared to the time between kicks and they produce a random phase change in the molecules having the collisions. The random phase changes lead to a decay in the average polarization plus a random polarization proportional to the square root of the number of molecules which have been dephased. The Langevin operator is included to account for this random polarization which turns out to be what is needed to maintain the operator properties of $\hat{Q}(z,t)$. In particular we do not want the operator to be completely damped out. As I will show this leads to a decay in the number of atoms in the system. Many of the ideas used in this section are similar to those presented by Lax[38]. To characterize the Langevin operator, its second moments will be calculated in this section. To calculate the second moments of $\hat{F}(z,t)$, assume that the atoms in a particular slice of the Raman medium at location z have been driven into an arbitrary superposition of levels 1 and 3 and then the driving fields are turned off at time t=0. Because no population damping has been included in the derivation of $\hat{Q}(z,t)$, one would expect that the number of atoms in levels 1 and 3 would remain unchanged. Collisions will cause the coherence to decay but do nothing to the number density of atoms in each level. The operators which give the fraction of atoms in levels 1 and 3 which are $\hat{\sigma}_{11}$ and $\hat{\sigma}_{33}$ which can be formed from $\hat{Q}(z,t)$ and $\hat{Q}^{+}(z,t)$ using

$$\hat{Q}^{+}(z,0)\hat{Q}(z',0)=\frac{\hat{\sigma}_{11}(z,0)\delta(z-z')}{\rho} \quad \text{and} \quad \hat{Q}(z,0)\hat{Q}^{+}(z',0)=\frac{\hat{\sigma}_{33}(z,0)\delta(z-z')}{\rho} \tag{2.57a}$$

which implies

$$\hat{Q}^{+}(z,t)\hat{Q}(z',t)=\frac{\hat{\sigma}_{11}(z,t)\delta(z-z')}{\rho} \quad \text{and} \quad \hat{Q}(z,t)\hat{Q}^{+}(z',t)=\frac{\hat{\sigma}_{33}(z,t)\delta(z-z')}{\rho} \quad . \tag{2.57b}$$

The operators $\hat{\sigma}_{11}$ and $\hat{\sigma}_{33}$ are defined analogous to Equation 2.25. When the driving fields are turned off, Equation 2.27 becomes

$$\frac{d\hat{Q}(z,t)}{dt}=-(\Gamma+i\Delta_e)\hat{Q}+\hat{F}(z,t) \tag{2.58}$$

which is formally integrated to give

$$\hat{Q}(z,t) = \hat{Q}(z,0)\exp[-(\Gamma + i\Delta_e)t] + \int_0^t \hat{F}(z,t')\exp[(\Gamma + i\Delta_e)(t'-t)]dt' \quad . \tag{2.59}$$

Next the expectation of the product $\hat{Q}^+(z,t_1)$ and $\hat{Q}(z,t_2)$ is calculated giving

$$\langle \hat{Q}^+(z,t_1)\hat{Q}(z',t_2)\rangle = \langle \hat{Q}^+(z,0)\hat{Q}(z',0)\rangle \exp[-\Gamma(t_1+t_2)]\exp[i\Delta_e(t_1-t_2)]$$

$$+\int_0^{t_2}\int_0^{t_1}\langle \hat{F}^+(z,t'_1)\hat{F}(z',t'_2)\rangle \exp[(\Gamma - i\Delta_e)(t_1'-t_1)]\ \exp[(\Gamma + i\Delta_e)(t_2'-t_2)]\ dt'_1 dt'_2 \quad . \tag{2.60}$$

At this point it is clear why the Langevin operator is needed. Without it the number of atoms in the ground state decays as $\exp(-2\Gamma t)$ and if the reverse ordering is calculated one finds that the number of atoms in state 3 also decays as $\exp(-2\Gamma t)$. The Langevin operator is added so that it exactly compensates for this unphysical decay and preserves probability.

Because the operators for different atoms are uncorrelated at t=0, the operators for different slices must also be initially uncorrelated. Using Equation 2.57 the initial second order moment of $\hat{Q}(z,t)$ is

$$\langle \hat{Q}^+(z,0)\hat{Q}(z',0)\rangle = \frac{\langle \hat{\sigma}_{11}(z,0)\rangle}{\rho}\delta(z-z') \tag{2.61}$$

where $\langle \hat{\sigma}_{11}(z,t)\rangle$ is the number density in state 1. For unequal times and the driving fields turned off, the second moment of $\hat{Q}(z,t)$ will have the form of

$$\langle \hat{Q}^+(z,t_1)\hat{Q}(z',t_2)\rangle = \frac{\langle \hat{\sigma}_{11}(z,t)\rangle}{\rho} g(t_1-t_2)\delta(z-z') \quad . \tag{2.62}$$

To determine the second order correlation for $\hat{F}(z,t)$, the form

$$\langle \hat{F}^{+}(z,t_1)\hat{F}(z',t_2)\rangle = D\,\delta\,(t_1-t_2)\;\delta(z-z') \tag{2.63}$$

is assumed and then shown to give the correct result when the constant D is properly chosen. With this assumption, Equation 2.60 becomes

$$g\,(t_1-t_2)\frac{\langle\hat{\sigma}_{11}(z,t)\rangle}{\rho} = \frac{\langle\hat{\sigma}_{11}(z,t)\rangle}{\rho}\exp[-\Gamma(t_1+t_2)]\;\exp[i\Delta_e(t_1-t_2)]$$

$$+\exp[\Delta_e(t_1-t_2)]\;\exp[-\Gamma(t_1+t_2)]\int_0^{t_2} D\,(z,t'_2)\exp(2\Gamma t'_2)\,dt'_2 \tag{2.64}$$

where the assumption $t_2 \geq t_1$ has been used. The approximation that $\langle\hat{\sigma}_{11}(z,0)\rangle = \langle\hat{\sigma}_{11}(z,t)\rangle \approx 1$ is now made and the assumption that D is constant is also used. For the special case of $t_2 = t_1$, equation 2.61 requires that $g \Rightarrow 1$ and the above equation can be solved for D to give $D = 2\Gamma/\rho$. Equation 2.63 then becomes

$$\langle \hat{F}^{+}(z,t_1)\hat{F}(z',t_2)\rangle = \frac{2\Gamma}{\rho}\delta(t_1-t_2)\;\delta(z-z') \quad . \tag{2.65}$$

A similar result is obtained for the opposite ordering with the substitution $\hat{\sigma}_{11} \Rightarrow \hat{\sigma}_{33}$ in Equation 2.64. For this case D is assumed to be slowly varying compared to $\exp(2\Gamma t')$ giving the antinormal ordered second moment of the Langevin operator

$$\langle \hat{F}(z',t')\hat{F}^{+}(z,t)\rangle = \frac{2\Gamma\langle\hat{\sigma}_{33}(z,t)\rangle}{\rho}\delta(z-z')\delta(t-t') \quad . \tag{2.66}$$

Now that the Langevin operator has been determined, the linear SRS equations can be solved.

Retarded Time Transformation

The coupled Equations 2.27 and 2.55 can be simplified by changing to the retarded time frame. The variable transformation is defined by[16]

$$\xi = z \qquad \tau = t - z/c \quad . \tag{2.67}$$

This is an unusual transformation because $\xi = z$. The partial derivative with respect to z transforms as

$$\frac{\partial}{\partial z} = \frac{\partial \xi}{\partial z}\frac{\partial}{\partial \xi} + \frac{\partial \tau}{\partial z}\frac{\partial}{\partial \tau} = \frac{\partial}{\partial \xi} - \frac{1}{c}\frac{\partial}{\partial \tau} \quad . \tag{2.68}$$

and the partial derivative with respect to t transforms as

$$\frac{\partial}{\partial t} = \frac{\partial \xi}{\partial t}\frac{\partial}{\partial \xi} + \frac{\partial \tau}{\partial t}\frac{\partial}{\partial \tau} = \frac{\partial}{\partial \tau} \quad . \tag{2.69}$$

Once this transformation has been made, the variable ξ will be replaced with z for simplicity. The above transformation has a simple physical interpretation. An observer at location z who measures the laser fields as a function of time picks $\tau = 0$ at the same place on the temporal pulse. This is not a relativistic transformation but rather a convenient choice of $t = 0$.

In the retarded time frame, the SRS Equations 2.27 and 2.55 become

$$\frac{d\hat{Q}(z,\tau)}{d\tau} = -\hat{Q}(z,\tau)(\Gamma + i\Delta_e) - i\kappa_1 \mathrm{E}_p(z,\tau)\hat{\mathrm{E}}_s^{(+)}(z,\tau) + \hat{F}(z,\tau) \tag{2.70}$$

and

$$\frac{\partial \hat{\mathrm{E}}_s^{(+)}(z,\tau)}{\partial z} = i\kappa_2 \hat{Q}(z,\tau)\mathrm{E}_p^*(z,\tau) \quad . \tag{2.71}$$

This transformation greatly simplifies the solution to the SRS equations.

Linear Solution

The coupled Equations 2.70 and 2.71 with the conditions given in Equations 2.61 and 2.65 have an exact solution. Note that the coupling is linear because the pump field is a prescribed input function which is not affected by the scattering process. The solution to these linear equations is [16]

$$\begin{aligned}\hat{\mathrm{E}}_s^{(-)}(z,\tau) = \hat{\mathrm{E}}_s^{(-)}(0,\tau) - i\kappa_2 \mathrm{E}_p(\tau)\exp(-\Gamma\tau)\int_0^z dz'\hat{Q}^+(z',0) I_0(\{(1-z'/z)q(0,\tau)\}^{1/2}) \\ + 2\kappa_1\kappa_2 z \mathrm{E}_p(\tau)\int_0^\tau d\tau' \exp[-\Gamma(\tau-\tau')]\,\mathrm{E}_p^*(\tau')\hat{\mathrm{E}}_s^{(-)}(0,\tau')\frac{I_1(\{q(\tau,\tau')\}^{1/2})}{q(\tau,\tau')^{1/2}} \\ - i\kappa_2 \mathrm{E}_p(\tau)\int_0^\tau d\tau' \int_0^z dz' \exp[-\Gamma(\tau-\tau')]\hat{F}^+(z',\tau') I_0(\{(1-z'/z)q(\tau,\tau')\}^{1/2})\end{aligned} \tag{2.72}$$

where the $I_n(x)$ are modified Bessel functions and

$$q(\tau_a,\tau_b) = 4\kappa_1\kappa_2 z \int_{\tau_b}^{\tau_a} |\,\mathrm{E}_p(\tau')\,|^2\, d\tau' \tag{2.73}$$

is the power of the pump laser field integrated from time τ_a up to time τ_b. Note that the pump field does not depend on z because it is not being depleted as it propagates. The above equation has been written for $\Delta_e = 0$. For the case of $\Delta_e \neq 0$ the Stokes field operator can be transformed so that Δ_e is eliminated in Equation 2.27.

Equation 2.72 is an important solution which has been used to understand many of the experiments involving SRS. It is a general solution because it can be integrated for an arbitrary initial Stokes seed and polarization. Once the initial conditions and the pump field is prescribed, the actual evaluation of this solution must be done on a computer. The linear solution is only valid before pump depletion. The SRS equations with pump depletion included are presented in the next section.

The Nonlinear Stimulated Raman Scattering Equations

The nonlinear SRS equations can be derived from the linear SRS equations by requiring energy conservation. Since the nonlinear equations will be used when the Stokes field is large enough to begin to deplete the pump, the operator equations can be converted to c-number equations. In addition, the Langevin term can be neglected. To go from operator equations to c-number equations the operators can simply be replaced with their corresponding classical analogues. To make the c-number equations simpler, I choose to make the following identification between the classical and quantum variables

$$Q(z,\tau) = \frac{i}{\kappa_1}\left(\frac{\omega_p}{\omega_s}\right)^{1/2} \hat{Q}(z,\tau) \quad \text{and} \quad \mathrm{E}_s^*(z,\tau) = \left(\frac{\omega_p}{\omega_s}\right)^{1/2} \hat{\mathrm{E}}_s^{(+)}(z,\tau) \quad . \tag{2.74}$$

Using this transformation, Equations 2.70 and 2.71 become the semiclassical equations

$$\frac{\partial Q(z,\tau)}{\partial \tau} = -Q(z,\tau)(\Gamma + i\Delta_e) + \mathrm{E}_p(z,\tau)\mathrm{E}_s^*(z,\tau) \tag{2.75}$$

and

$$\frac{\partial \mathrm{E}_s^*(z,\tau)}{\partial z} = \kappa_1\kappa_2 Q(z,\tau)\mathrm{E}_p^*(z,\tau) \quad . \tag{2.76}$$

The energy conservation condition can be written as

$$\mathrm{E}_p(z,\tau)\mathrm{E}_p^*(z,\tau) + \mathrm{E}_s(z,\tau)\mathrm{E}_s^*(z,\tau) = \Psi(\tau) \tag{2.77}$$

where $\Psi(\tau)$ is the power in the input pump pulse. Differentiating with respect to z and using Equation 2.76 and its complex conjugate we have

$$\mathrm{E}_p^*(z,\tau)\left\{\frac{\partial \mathrm{E}_p(z,\tau)}{\partial z} + \kappa_1\kappa_2 \mathrm{E}_s(z,\tau)Q(z,\tau)\right\} = -\mathrm{E}_p(z,\tau)\left\{\frac{\partial \mathrm{E}_p^*(z,\tau)}{\partial z} + \kappa_1^*\kappa_2^*\,\mathrm{E}_s^*(z,\tau)Q^*(z,\tau)\right\} \tag{2.78}$$

The left hand side of this equation is the negative complex conjugate of the right hand side so both sides are pure imaginary. Because E_p starts out being an arbitrary complex input field the only way the above equation can generally be satisfied is for the bracketed quantities to be identically zero which gives the third SRS equation

$$\frac{\partial E_p(z,\tau)}{\partial z} = -\kappa_1\kappa_2 E_s(z,\tau)Q(z,\tau) \quad . \tag{2.79}$$

The set of Equations 2.75, 2.76, and 2.79 form the set of semiclassical nonlinear SRS equations. This system of equations is nonlinear because the pump field is now a dynamical variable and thus the Q equation contains products of dynamical variables.

No general solution exists for the set of nonlinear SRS equations. However, there does exist an interesting class of special solutions in the hypertransient limit where the pulses are short compared to the dephasing time of the medium. Because they are a special set of solutions, one would expect that they could only be realized by using a special set of initial conditions. As will be discussed in Chapter 3, the special conditions can be experimentally generated.

The Soliton Solution

For the linear region, a general solution was given in Equation 2.72. This means that for an arbitrary input pump and Stokes fields, the field can be evaluated at any z for all τ. However, evaluation still includes integration over the initial conditions with the appropriate Green's function. The soliton solution is an exact solution for a particular set of input pump and Stokes fields for the hypertransient regime where the duration of the fields is short compared to the collisional dephasing time. So if just the right fields are injected into a Raman amplifier, the fields at any location z can easily be evaluated. The form of the soliton solution is sech(τ) for the pump field and tanh(τ) for the Stokes field. It is not easy to generate this particular form for the input fields. However, due to damping, these special temporal shapes can be approximated in the amplifier when a π phase shift is present in the input Stokes seed.

Before presenting the soliton solution, a variable transformation will be performed to simplify the differential equations. To account for detuning, new variables for the Stokes field are defined by[32]

$$Q(z,\tau) = \chi(z,\tau)\exp[-i\Delta_e\tau] \qquad (2.80)$$

and

$$E_s(z,\tau) = A_s \exp(i\Delta_e\tau) \quad . \qquad (2.81)$$

With this transformation, the SRS equations are transformed to

$$\frac{\partial\chi(z,\tau)}{\partial\tau} = -\Gamma\chi(z,\tau) + E_p(z,\tau)A_s^*(z,\tau) \quad , \qquad (2.82)$$

$$\frac{\partial A_s(z,\tau)}{\partial z} = \kappa_1\kappa_2\,\chi^*(z,\tau)E_p(z,\tau) \quad , \qquad (2.83)$$

and

$$\frac{\partial E_p(z,\tau)}{\partial z} = -\kappa_1\kappa_2\,\chi(z,\tau)A_s(z,\tau) \quad . \qquad (2.84)$$

This transformation makes the SRS equations appear to be on resonance. In fact, looking at these equations, one might ask why a Stokes seed, which is off resonance, evolves any differently than a seed which is on resonance. The answer lies in the fact that $A_s(z,0)$ has a phase which oscillates as $\exp(-i\Delta_e\tau)$. Therefore, the first part of the Stokes field will generate an oscillation in the medium, which is not at the optimum phase, for the growth of the subsequent portions of the Stokes field. The exact soliton solution to the coupled SRS equations only holds for pulses which are short compared to Γ so that the damping term can be neglected. In other words, the soliton pulse passes through a slice of the medium before significant collisional dephasing occurs. In this limit a solution to the SRS equations is

$$E_p = E_{po}\operatorname{sech}(\alpha) \tag{2.85}$$

$$A_s = E_{po}\exp(ib)\tanh(\alpha) \tag{2.86}$$

$$\chi = -W\, E_{po}^2 \exp(-ib)\operatorname{sech}(\alpha) \tag{2.87}$$

where

E_{p0}= amplitude of the soliton

T= characteristic width of the soliton

b = arbitrary phase between pump and Stokes and

$$\alpha = \frac{\tau - \tau_0}{W} - W\, E_{p0}^2(z - z_0)\,\kappa_1\kappa_2 \quad . \tag{2.88}$$

This solution can easily be verified by noting that

$$\frac{d\,\mathrm{sech}(\alpha)}{dz} = -\mathrm{sech}(\alpha)\tanh(\alpha)\frac{d\alpha}{dz} \text{ and } \frac{d\tanh(\alpha)}{dz} = \mathrm{sech}^2(\alpha)\frac{d\alpha}{dz} \quad . \tag{2.89}$$

The soliton solution for the Stokes field given in Equation 2.86 does not allow for an oscillation at Δ_e. This means that the soliton solution forces the Stokes field to be on resonance. The above solution holds for $\Gamma = 0$; solutions have also been found which are correct to first order in Γ[31,32]. For these solutions the soliton narrows approximately as

$$W = (z + a)^{-1/2} \tag{2.90}$$

where a is a constant depending on the width at $z = 0$. The amplitude of the soliton does not decay for this solution. The soliton solution will be revisited in Chapter 6.

Steady State Solution

If the slowly varying envelopes of the pump and Stokes fields are restricted to vary slowly compared to the dephasing time ($1/\Gamma$), the solution to the system of nonlinear SRS equations can be greatly simplified. If the field envelopes change slowly compared to ($1/\Gamma$), then the quadrupole oscillation in the medium $Q(z,\tau)$ will always be nearly in equilibrium with the driving fields. This situation can be described intuitively as follows: the oscillation in the medium cannot remember far enough into the past to notice that the fields are not constant. This limit is called the steady state regime. Mathematically it is stated as

$$\frac{\partial Q}{\partial \tau} = 0 \quad . \tag{2.91}$$

Applying the steady state condition to Equation 2.75, we have

$$\Gamma Q(z,\tau) = \mathbf{E}_p(z,\tau)\mathbf{E}_s^*(z,\tau) \quad . \tag{2.92}$$

Note that $\Delta_e = 0$ has been assumed. If Δ_e is not zero, the Stokes field will pick up an oscillation and if the period of this oscillation is not longer than the dephasing time, the steady state solution would not apply. Substituting $Q(z,\tau)$ from Equation 2.92 into Equations 2.76 and 2.79, the SRS equations become

$$\frac{\partial \mathbf{E}_s^*(z,\tau)}{\partial z} = \frac{\kappa_1\kappa_2}{\Gamma}|\mathbf{E}_p(z,\tau)|^2\mathbf{E}_s^*(z,\tau) \tag{2.93}$$

and

$$\frac{\partial \mathbf{E}_p(z,\tau)}{\partial z} = -\frac{\kappa_1\kappa_2}{\Gamma}|\mathbf{E}_s(z,\tau)|^2\mathbf{E}_p \quad . \tag{2.94}$$

Multiplying the first equation by $2\mathbf{E}_s$ and the second by $2\mathbf{E}_p^*$, equations for the pump and Stokes intensities are formed which are

$$\frac{\partial \mathbf{I}_s(z,\tau)}{\partial z} = \frac{2\kappa_1\kappa_2}{\Gamma}\mathbf{I}_p(z,\tau)\mathbf{I}_s(z,\tau) \text{ and } \frac{\partial \mathbf{I}_p(z,\tau)}{\partial z} = -\frac{2\kappa_1\kappa_2}{\Gamma}\mathbf{I}_p(z,\tau)\mathbf{I}_s(z,\tau) \quad . \tag{2.95}$$

In the steady state regime, only the intensities are important so no transient asymmetry will be seen between the front and back of a partially depleted temporal pump pulse. The steady state equation can be simplified by the energy conservation requirement

$$\mathbf{I}_p(z,\tau) + \mathbf{I}_s(z,\tau) = \Psi(\tau) \quad . \tag{2.96}$$

This requirement reduces the system of equations to a single differential equation for the Stokes intensity which is

$$\frac{d\mathbf{I}_s(z,\tau)}{dz} = \frac{2\kappa_1\kappa_2}{\Gamma}\mathbf{I}_s(z,\tau)\,[\Psi(\tau) - \mathbf{I}_s(z,\tau)] \quad . \tag{2.97}$$

Separating the z and τ dependence and then integrating, we obtain

$$\int_{\mathbf{I}_s(0,\tau)}^{\mathbf{I}_s(z,\tau)} \frac{d\mathbf{I}_s}{\mathbf{I}_s(\Psi(\tau) - \mathbf{I}_s)} = 2\kappa_1\kappa_2 \int_0^z dz \quad . \tag{2.98}$$

Performing the integral using the integration formula[42]

$$\int \frac{dx}{x(a-x)} = -\frac{1}{a}\ln\left(\frac{a-x}{x}\right) \tag{2.99}$$

and evaluating at the limits gives

$$\exp[-\Psi(t)\kappa_1\kappa_2 z/\Gamma] \quad = \quad \left[\frac{\Psi(\tau) - \mathbf{I}_s(z,\tau)}{\mathbf{I}_s(z,\tau)}\right] \;/\; \left[\frac{\Psi(\tau) - \mathbf{I}_s(0,\tau)}{\mathbf{I}_s(0,\tau)}\right] \quad . \tag{2.100}$$

Solving for $I_s(z,\tau)$ the steady state solution is obtained which is[37]

$$I_s(z,\tau) = \frac{I_s(0,\tau)\Psi(\tau)}{I_s(0,\tau) + [\Psi(\tau) - I_s(0,\tau)]\exp[-\Psi(\tau)\kappa_1\kappa_2 z/\Gamma]} \quad . \tag{2.101}$$

Notice that the intensities at (z,τ_0) only depend on the input intensities at $(0,\tau_0)$ where τ_0 is any particular retarded time. The steady state solution is appropriate for many situations and it also serves as a simple slowly varying limit test for numerical integration which can treat more general problems.

In the following chapters, procedures for evaluating the solutions to the SRS equations will be developed and the results will be compared to experimental data. For treating the formation of solitons from a π phase shift in the Stokes seed, the nonlinear SRS equations must be integrated numerically.

CHAPTER 3

THEORY OF QUANTUM INITIATION AND AMPLIFICATION

In this chapter, the details of quantum initiation and the subsequent amplification through the linear regime will be discussed. First, quantum initiation in general for the Raman system will be discussed. In the following two sections, the theoretical and numerical details of generating coherent modes are discussed. Next, the method used to propagate the fields through pump depletion and the results at the end of depletion are presented. Finally, the c-number approach to calculating an output Stokes field will be discussed.

Quantum Initiation

There are two distinct ways of treating the quantum initiation of the Stokes pulse. One method is the c-number[11,38] approach which replaces the operator equations with classical variables including a randomly fluctuating Langevin force. The second method is the coherent modes approach[17]. For this method, the field operators are used to calculate the two-time correlation function from which individual Stokes pulses can be generated. Although the two methods are very different, the final results appear to be identical. In order to treat quantum initiation, one must begin with the quantum SRS equations. The solution given in Equation 2.72 can be used or the differential equations can be integrated numerically starting with the initial condition of no photons in the Stokes field. Due to the quantum nature of the initiation process, the output Stokes field will be different each time it is calculated. To simulate the initiation process, computer generated random numbers will be used. Average properties of the Stokes field can be calculated by generating an ensemble of pulses and averaging the data from the members together. If average quantities are desired before pump depletion, they can be calculated directly using the coherent modes approach.

The reason that the Raman scattering and related processes generate large fluctuations in the macroscopic fields is that there is a free phase that must be picked by the spontaneously emitting atoms. The pump field has a well defined phase but the phase of the Stokes field is completely random from shot to shot. Once the phase of the Stokes field has been picked it determines the phase of the quadrupole oscillation in the medium. If one thinks in terms of the wave function for a given mode of the field, there is no coherent driving force to lock the phases of adjacent number state contributions. As a result, each number state contribution to the wave function for the electric field has a random phase. This is part of what is needed to produce a chaotic state of light. Spontaneous emission does in fact produce chaotic states of light which have the following distribution of number states[18]

$$P(n) = \frac{\overline{n}^{n}}{(1+\overline{n})^{1+n}} \tag{3.1}$$

where $\overline{n}$ is the ensemble average number of photons in the mode. Two examples of this distribution are shown in Figures 2 and 3 along with coherent states having the same average number of photons. The photon number probability distribution for coherent states is

$$P(n) = \frac{\bar{n}^n}{n!}\exp(-\bar{n}) \quad . \tag{3.2}$$

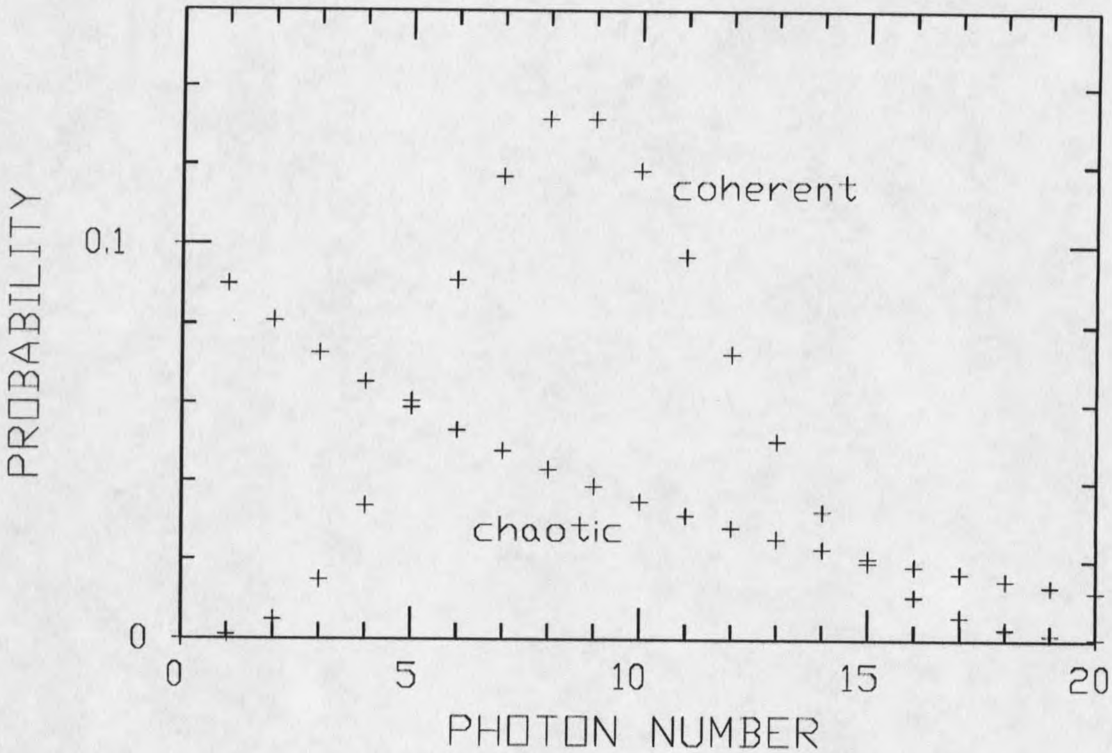

Figure 2 Photon number probability distribution for a coherent and chaotic state having an average of nine photons. Chaotic state is approximately a decaying exponential and the coherent state is approaching a gaussian distribution.

The number state contributions to a coherent state are all phase locked, meaning that they all have a phase of zero at some time which could be labeled $t=0$. Note from Figure 3 that even for large values of $\bar{n}$ the number of photons in a chaotic state can vary wildly which would result in wild fluctuations in measurements of the energy in the mode. This large uncertainty can also lead to large fluctuations in the spectrum when more than one significantly excited mode is present in a Stokes pulse. This is because the relative phases of the modes are random and thus they will beat together in a random way to produce spectral fluctuations when the Fourier transform is taken.

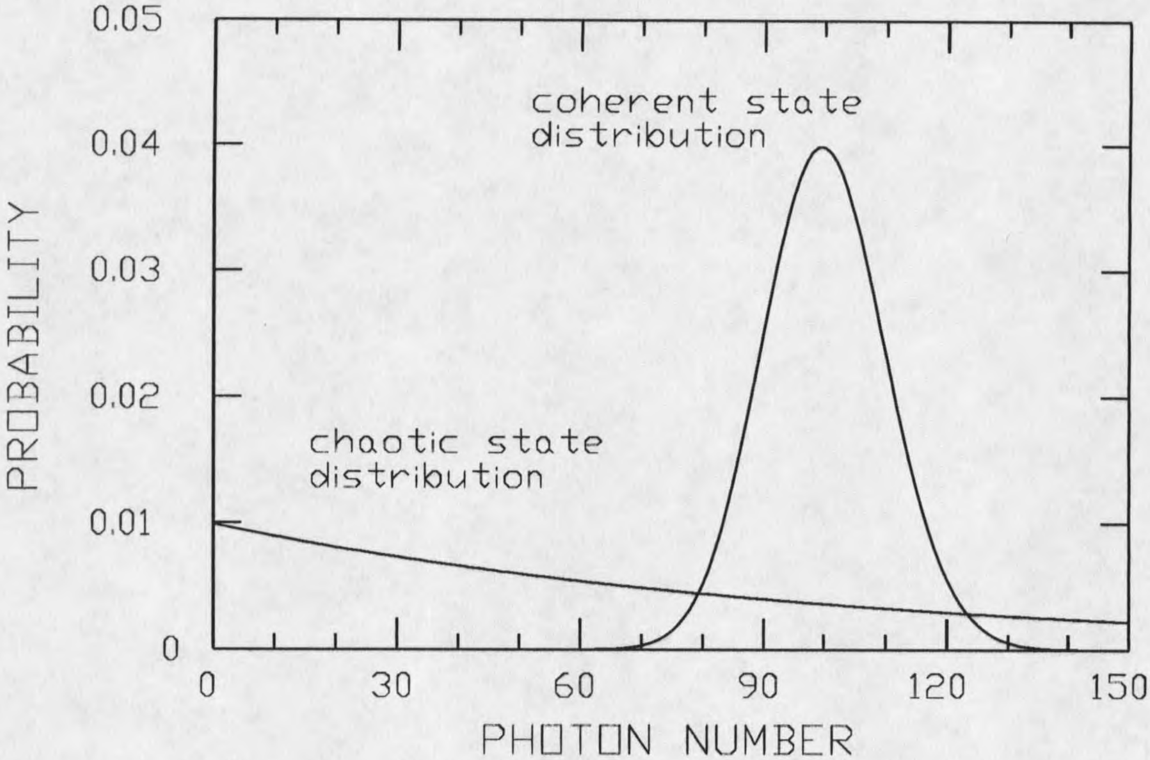

Figure 3 Photon number probability distribution for a coherent and a chaotic state having an average of 100 photons. Even for highly excited modes the number of photons in a chaotic state can have a large range of values. The coherent state distribution becomes narrow compared to the average number of photons.

In order to carry out a calculation to generate a member of the output Stokes field, one needs to decide what to specify for the initial conditions for $\hat{Q}(z,0)$ and $E_s(0,\tau)$ and for the magnitude of the Langevin fluctuations. The choice will depend on whether in the final result one calculates normal ordered quantities or antinormal ordered quantities. Since detectors measure intensity, which is a normal ordered quantity, one should use normal ordering. The ordering is important when calculating low level intensities where a difference of one photon is significant. However, at the end of the Raman generator, the fields are quite large and thus classical so that the difference between the two orderings is expected to be extremely small. For normal ordering, one can use the square root of $\langle \hat{Q}^{+}(z,0) \quad \hat{Q}(z,0)\rangle$, $\langle \hat{a}^{+}(0,\tau) \quad \hat{a}(0,\tau)\rangle$, and $\langle \hat{F}^{+}(z,\tau) \quad \hat{F}(z,\tau)\rangle$ to determine the magnitude of the fluctuations. The reverse operator ordering is used for the antinormal ordered approach.

When using normal ordering, there is no contribution from the vacuum field but there are contributions from $\hat{Q}(z,0)$ and $\hat{F}(z,\tau)$. The initial linear number density can be expressed as $\langle \hat{Q}^{+}(z,0) \quad \hat{Q}(z,0)\rangle$. However, for times large compared to $1/\Gamma$, the contribution from $\hat{Q}(z,0)$ decays as can be seen from Equation 2.72. This is unphysical because one would expect that an initial polarization fluctuation in the medium would be amplified as the laser pulse passes, leading to a substantial Stokes field for most of the pulse duration. This problem arises because of the way we have phenomenologically included damping. To maintain consistency, a Langevin term is added. For normal ordering, $\langle \hat{F}^{+}(z,\tau) \quad \hat{F}(z,\tau)\rangle$ is found from Equations 2.65 and 2.66 to be proportional to the linear number density of the atoms in the ground state. This "large" Langevin force generates a contribution in the last term of Equation 2.72 which properly accounts for the initial polarization fluctuations plus the polarization fluctuations occurring after $\tau = 0$. On the other hand if one chooses to use antinormal ordering, there is no contribution from $\langle \hat{Q}(z,0) \quad \hat{Q}^{+}(z,0)\rangle$ but there is a contribution from the vacuum field. In addition, the expectation value from the Langevin force, $\langle \hat{F}(z,\tau) \quad \hat{F}^{+}(z,\tau)\rangle$, is now "small" and proportional to the linear density of atoms in the excited state $|3\rangle$. This Langevin force preserves the number of atoms in state $|3\rangle$ in the absence of driving fields. Since the fraction of atoms in state $|3\rangle$ is quite small, one would expect that the contribution from the Langevin term would also be small.

When performing a c-number calculation, it is advantageous to use antinormal ordering because as we will show the Langevin term can in fact be neglected. This has also been verified by Englund[36]. Omitting the Langevin term greatly decreases the computing time because this term contains a double integral. To show that the Langevin term can be omitted when using the antinormal ordered approach to calculate large field amplitudes, we performed the c-number calculation without the Langevin force and then compared the results with those obtained from the normal ordered coherent modes theory.

We initiate Raman scattering by including random noise in the initial Stokes field. Since the final Stokes field is much larger than the initiating noise the first of the four terms in Equation 2.72 can be ignored leaving only the third term. To generate an ensemble member, the operators were replaced with c-number variables. As with the coherent modes approach, this equation is only valid in the linear regime before pump depletion. The fields resulting from the c-number analog of Equation 2.72 are used as the inputs in the semiclassical nonlinear equations for propagation through depletion.

Coherent Mode Expansion

In order to perform a fully quantum mechanical calculation, the radiation field must somehow be broken up into modes. There appears to be an infinite number of ways to do this. For example, one could begin with modes defined using periodic boundary conditions and then make an arbitrary rotation in Hilbert space. We want to choose the mode expansion which makes the calculation simplest. The coherent modes expansion simplifies the calculation by requiring that the modes are completely independent[17].

Before describing the coherent mode theory in more detail, a few points should be made about the theory. For a given location in the Raman medium, the coherent modes are identical for all shots. Therefore the magnitude of the complex degree of coherence[43] has a maximum value of one for the individual modes. Fluctuations occur because of variations in the level of excitation and phase of each mode from shot to shot. Quantum initiation is included through both a Langevin noise operator associated with collisional damping and by an initial polarization in the medium. The initial polarization is included because the atomic coherence operator does not commute with the atomic inversion operator. Therefore, one cannot specify both that the system starts in the ground state and that the initial polarization is zero. As a possible physical picture, imagine that one measures the polarization of an ensemble of single hydrogen molecules which are prepared in their ground state. Each molecule would have a finite polarization with an average order of magnitude of $e\, a_o$. However, if the polarization of a sample of hydrogen gas is measured, the magnitude of the resulting polarization per atom would be proportional to $\sqrt{N}/N$ due to random orientations. This simple model gives the correct magnitude of the fluctuating polarization which initiates the stimulated emission. For combination of normal and antinormal ordering, the spontaneous emission can be attributed to a combination of vacuum field fluctuations and polarization fluctuations.[10,23,24]

An appealing feature of using the coherent modes approach is that the q-number equations are not replaced with stochastic c-number equations. Instead, the operator equations are used to calculate the two-time coherence function which depends only on expectation values of the system and Langevin operators. Once the correlation function is calculated for a given gain and location in the Raman generator, it is used to generate the temporal coherent modes. Next, a particular realization of the electric field is formed by adding these modes together with random phases and gaussian amplitude statistics. This can be done many times to generate an ensemble of temporal Stokes pulses. Since this is the last stage of the calculation before depletion, it is easy to generate a large ensemble which can be used to calculate statistics.

The two-time correlation function for a single transverse Stokes mode is defined in terms of the normal ordered field operators as

$$G(\tau_1,\tau_2) = \frac{c}{2\pi\hbar\omega_s}\langle \hat{\mathrm{E}}_s^{(-)}(z,\tau_1)\hat{\mathrm{E}}_s^{(+)}(z,\tau_2)\rangle \quad . \tag{3.3}$$

Note that the coherence function and thus our choice of modes depends on the location z where the modes are evaluated. When the solution to the linear SRS equation given in Equation 2.72 and its complex conjugate are substituted into the above equation, the two time correlation functions becomes

$$\begin{aligned} G(\tau_1,\tau_2) = {} & \frac{c\kappa_2\kappa_2^*}{2\pi\hbar\omega_s}\mathrm{E}_p(\tau_1)\mathrm{E}_p^*(\tau_2)\exp[-\Gamma(\tau_1+\tau_2)] \\ \times & \left\{\int_0^z dz'\int_0^z dz''\langle\hat{Q}^+(z',0)\hat{Q}(z'',0)\rangle\ \mathrm{I}_0([q(\tau_1,0)(1-z'/z)]^{1/2})\,\mathrm{I}_0([q(\tau_2,0)(1-z''/z)]^{1/2})\right. \\ + & \ \kappa_2\kappa_2^*\,\mathrm{E}_p(t_1)\mathrm{E}_p^*(\tau_2)\int_0^{\tau_2}d\tau'_2\int_0^{t_1}d\tau'_1\int_0^z dz'\int_0^z dz''\exp(-\Gamma[(\tau_1-\tau'_1)+(\tau_2-\tau'_2)]) \\ \times & \left.\langle\hat{F}^+(z',\tau'_1)\hat{F}(z'',\tau'_2)\rangle\,\mathrm{I}_0([q(\tau_1,\tau'_1)(1-z'/z)]^{1/2})\,\mathrm{I}_0([q(\tau_2,\tau'_2)(1-z''/z)]^{1/2})\right\} \end{aligned} \tag{3.4}$$

where $\tau_2 \geq \tau_1$ has been assumed and the integrated pump intensity from τ_b up to τ_a has been written as

$$q(\tau_a,\tau_b) = 4\kappa_1\kappa_2 z\int_{\tau_b}^{\tau_a}|\mathrm{E}_p(\tau')|^2 d\tau' \quad . \tag{3.5}$$

Using Equations 2.61 and 2.65, the correlation function becomes

$$G(\tau_1,\tau_2)=\frac{c\,\kappa_2\kappa_2^*}{2\pi\hbar\omega_s}\mathrm{E}_p(\tau_1)\mathrm{E}_p^*(\tau_2)\exp[-\Gamma(\tau_1+\tau_2)]\,\frac{2}{\rho}\left\{\int_0^z \mathrm{I}_0([q(\tau_1,0)\,(1-z'/z)]^{1/2})\right.$$

$$\times\quad \mathrm{I}_0([q(\tau_2,0)\,(1-z'/z)]^{1/2})dz'+2\Gamma\int_0^{\tau_2}d\tau'_2\int_0^z dz'\exp(-2\Gamma\tau'_2)$$

$$\left.\times\quad \mathrm{I}_0([q(\tau_1,\tau'_2)\,(1-z'/z)]^{1/2})\,\mathrm{I}_0([q(\tau_2,\tau'_2)\,(1-z'/z)]^{1/2})\right\}\quad . \tag{3.6}$$

To evaluate the integrals over z', the following integration formula is used[42]

$$\int_0^x du\;u\;\mathrm{I}_n(\alpha u)\mathrm{I}_n(\beta u)=\frac{x}{\alpha^2-\beta^2}\{\alpha\,\mathrm{I}_n(\beta x)\mathrm{I}'_n(\alpha x)-\beta\,\mathrm{I}_n(\alpha x)\mathrm{I}'_n(\beta x)\} \tag{3.7}$$

where the derivative of the modified Bessel function of order zero is given by

$$\mathrm{I}'_0(x)=\mathrm{I}_1(x)\quad . \tag{3.8}$$

To get Equation 3.6 in the desired form, the following variable transformation is made

$$u=\left(1-\frac{z'}{z}\right)^{1/2}\qquad du=-\frac{1}{2}\frac{dz'}{u}\ \text{and}\ u(z'=0)=1\qquad u(z'=z)=0\quad . \tag{3.9}$$

Evaluating the z' integrals and normalizing the correlation function so that $G(\tau_c,\tau_c)=1$ where τ_c is the center of the laser temporal pulse, the two time correlation function is

$$G(\tau_1,\tau_2)=\frac{E_p(\tau_1)E_p^*(\tau_2)}{2\,|E_{(\tau_c)}|^2\,q(\tau_1,\tau_2)}e^{-\Gamma(\tau_1+\tau_2)}\left[f(\tau_1,\tau_2)+2\Gamma\int_0^T e^{2\Gamma\tau'}g(\tau')d\tau'\right] \tag{3.10}$$

where

$$f(\tau_1,\tau_2)=[q(\tau_1,0)]^{1/2}\,I_1([q(\tau_1,0)]^{1/2})\,I_0([q(\tau_2,0)]^{1/2})-(1\leftrightarrow 2)\quad ,$$

$$g(\tau')=[q(\tau_1,\tau')]^{1/2}\,I_1([q(\tau_1,\tau')]^{1/2})\,I_0([q(\tau_2,\tau')]^{1/2})-(1\leftrightarrow 2)\quad . \tag{3.11}$$

The symbol $(1 \leftrightarrow 2)$ indicates interchange of τ_1 and τ_2 and the condition that $\tau_2 \geq \tau_1$ has been replaced by the condition that T is the smaller of τ_1 and τ_2. Since the overall amplitude of the correlation function is not of particular interest here, there are only two free parameters to choose once the pump field has been prescribed. The first parameter is the gain times the length of the medium which is $(4\ k_1\ k_2\ z)$ and the second parameter is the Raman linewidth (Γ). The Raman linewidth can be calculated from the pressure of the hydrogen in the Raman cell. The experiments that were done used pressures between 10 and 32 atmospheres of H_2. The collisional dephasing rate was measured by Bischel[13] and found to be 52.2MHz per amagat.

Since the temporal pulse shape from our laser is nearly gaussian and the pulse is single mode, we approximated $E_p(\tau)$ by a normalized gaussian times an amplitude E_0

$$E_p(\tau)=\frac{E_0}{\sqrt{\sigma\sqrt{\pi}}}\exp\left[-\frac{(\tau-\tau_c)^2}{2\sigma^2}\right]\quad . \tag{3.12}$$

Experimentally the $1/e$ width σ of the temporal intensity is 15nsec giving a Full Width Half Max (FWHM) of 26nsec. This leaves the quantity $\beta \equiv 4k_1k_2E_0^2z$ as an adjustable parameter. The value of β was determined by varying it until the calculated average gain narrowed linewidth agreed with that obtained experimentally. In the coherent mode theory, the average linewidth is found by evaluating the coherence function at equal times. However, experimentally we measured the linewidth after pump depletion and the coherent modes theory is only valid before depletion. If the linewidth does not change significantly through depletion (as we will show is the case) our method for obtaining β is valid. We found that β=10000 (which corresponds to a normal steady state peak gain of $G_{ss} \equiv 4k_1k_2zE_L^2(\tau_c)/2\Gamma = 38$) gave good agreement with the experimental linewidth of approximately 210MHz.

Once the two time correlation function is determined from the Heisenberg equations of motion, we need to relate it to an orthonormal set of temporal modes. To accomplish this, the field operators $\hat{E}_s^{(+)}$ and $\hat{E}_s^{(-)}$ are expressed as an expansion in coherent modes

$$\hat{E}_s^{(-)}(z,\tau) = \left[\frac{2\pi\hbar\omega_s}{c}\right]^{1/2} \sum_n \hat{b}_n^{+}\psi_n(\tau) \tag{3.13}$$

where $\hat{b}_n^{+}$ is the creation operator for the nth coherent mode and $\hat{E}_s^{(+)}$ is given by the hermitian conjugate of Equation 3.13. Do not confuse the $\hat{b}_n^{+}$ with the $\hat{a}_n^{+}$ operator for cavity modes. The coherent modes, $\Psi_n(\tau)$, are localized modes which are not confined to a box. Unlike cavity modes, the coherent modes will evolve in z. The simplifying feature of using coherent modes is that the level of excitation of one coherent mode is independent of the level of excitation of all other coherent modes. This would not be the case if the radiation field was expressed in the cavity mode basis. For the cavity mode expansion, the Stokes field would become a complicated superposition of correlated modes. Because the coherent modes are independent, their level of excitation can be calculated one at a time. When the pump begins to deplete, the coherent modes become correlated because they compete for pump photons. In other words, all the modes cannot decide to be highly excited on the same shot.

Below pump depletion, the Raman equations are linear and the coherent modes evolve independently. Since the phases of the modes are statistically independent, the cross terms will drop out when Equation 3.13 is inserted into Equation 3.3 to relate the coherent modes to the correlation function. With the definition $\lambda_n = \langle a_n^+ a_n \rangle$, the correlation function is

$$G(\tau_1, \tau_2) = \sum_n \lambda_n \psi_n(\tau_1) \psi_n(\tau_2) \quad . \tag{3.14}$$

Using the orthonormality of the modes, Equation 3.14 can be converted to the integral equation

$$\int_{-\infty}^{+\infty} G(\tau, \tau') \psi_n(\tau') d\tau' = \lambda_n \psi_n(\tau) \quad . \tag{3.15}$$

This integral is well defined for a pulsed laser because $G(\tau, \tau + \Delta) \Rightarrow 0$ as $\Delta \Rightarrow \infty$. To solve this integral equation for the temporal modes, $G(\tau_1, \tau_2)$ and $\psi_n(\tau)$ were converted to discrete functions of time and the integral was replaced by a sum. The resulting eigenvalue equation was then solved on an AT&T 6300 plus micro computer using a standard routine from Argonne National Lab. We divided time into 89 steps and the resulting eigenvalue problem took about three minutes to solve. The solution vectors are the desired temporal modes and the corresponding eigenvalues give the average level of excitation of the mode. A list of the first fifteen eigenvalues are given in Table 1 and the first three modes are plotted in Figure 4.

Qualitatively, the modes look very much like harmonic oscillator wave functions. In analogy, with harmonic oscillator wave functions, the higher order modes are weighted

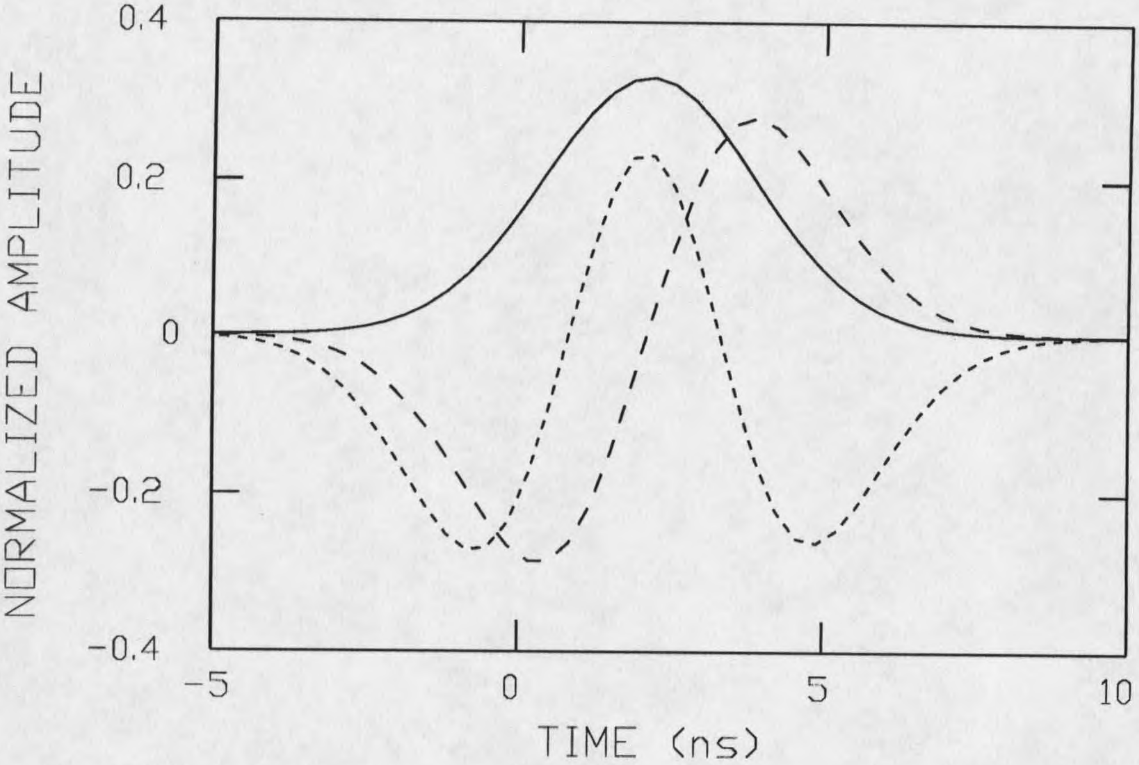

Figure 4 First three temporal modes generated using coherent modes theory. The modes resemble harmonic oscillator functions. Higher modes are weighted more on the temporal wings. The input gaussian pump pulse was centered at t=0.

more on the temporal wings. This will become important when the fields are propagated through depletion. The characteristic ratio $\Gamma\sigma/gz$ which indicates the number of significantly excited modes is also shown in Table 1.

A mode that grows from spontaneous emission without saturation will have a chaotic number state distribution with random phases between the number states. The chaotic state arises because populating a mode by a process without a preferential phase is analogous to a two dimensional random walk problem. For the random walk, the most probable final position is the starting point. Because the amount of phase space increases with the distance from the initial state, which is the ground state, the probability distribution for $|b_n|$ is

$\Gamma\sigma/gz$	n	λ_n
1.9	1	0.587
	2	0.2376
	3	0.994(-1)
	4	0.428(-1)
	5	0.189(-1)
	6	0.860(-2)
	7	0.401(-2)
	8	0.191(-2)
	9	0.935(-3)
	10	0.468(-3)
	11	0.239(-3)
	12	0.125(-3)
	13	0.663(-4)
	14	0.360(-4)
	15	0.199(-4)

Table 1 Statistical weights for the 15 dominant coherent modes. The value of $\Gamma\sigma/gz$ indicates the number of significantly excited modes.

$$P(|b_n|) = 2\frac{|b_n|}{\lambda_n} \exp\left[\frac{-|b_n|^2}{\lambda_n}\right] \quad . \tag{3.16}$$

The above equation is not valid for weakly excited modes. For weakly excited modes, Equation 3.1 must be used. To generate the complex fields for a member of the ensemble, the modes are added together each with a random phase uniformly distributed between 0 and 2π and with an amplitude distribution given in the above equation. Do not confuse this distribution with the probability distribution for the number of photons which is $P(|b|^2)$. The photon number distribution has the form of a decaying exponential for highly excited modes.

To generate random amplitudes for $|b_n|$, we calculated the required mapping which turned out to be

$$| b_n | = \sqrt{-\lambda_n \ln(1-x)} \tag{3.17}$$

where x is a random number with constant probability density between 0 and 1. Thus the computer picked an x and the calculated $| b_n |$ was used as the amplitude of the nth mode. At this point, we have a prescription for generating an ensemble of pulses before depletion without ever converting the q-number equations to c-number equations.

Numerical Procedure for Coherent Modes Calculation

To numerically calculate the coherent modes, the continuous variable τ must be replaced by a discrete set of τ_i's and the continuous functions $G(\tau_1, \tau_2)$ and $\psi_n(\tau)$ are replaced by discrete functions. The integral in Equation 3.15 is replaced by a sum and thus the integral equation becomes a matrix eigenvalue equation which can be solved numerically.

A computer program named GBUILD.BAS which calculates the discrete two-time correlation function was written using QUICK BASIC 4.0. This program and others used to generate the coherent modes are listed in Appendix B. In this program, the temporal input pump profile is assumed to be gaussian. The information which must be supplied to the program is:

Characteristic width of the pump envelope

Range of τ for which the correlation function is to be calculated

Temporal location of the center of the pump pulse

Raman linewidth in rad/sec at Half Width Half Max (HWHM)

Raman gain in the form of $2\sqrt{\kappa_1\kappa_2 z}$

Number of discrete steps of τ_i

The eigenvalues and eigenvectors of the correlation matrix were found by using routines from Argonne National Labs which are called by the program named EIGCALL.FOR. The vectors are stored in the file VECT.DAT and the eigenvalues are saved in EVAL.DAT.

Once the eigenvalues and eigenvectors are calculated, they are used to generate an ensemble of fields at the end of the linear region. Each member of this ensemble is used as an input seed for the nonlinear propagation through depletion. A three hundred member ensemble was used for calculating the average two time spectral correlation function. The ensemble members were generated and analyzed fifteen members at a time. A batch file named LOOP.BAT was used to run the various necessary programs. A flow chart of the procedure is shown in Figure 5. The final results are saved in the three files: COR.DAT, COR1.DAT, and COR2.DAT. These files have three columns of numbers. The first column labels the frequency, the second column is the spectral correlation function and the third column is the average spectral line. The file COR1.DAT contains the spectral data before depletion. The spectral data after depletion is saved in COR2.DAT and the data after being convolved with an instrument function is saved in the file COR.DAT.

Numerical Propagation Through Depletion

For both the coherent modes and c-number calculations, each member of the ensemble of Stokes pulses that was generated using Equation 2.72 was used as a Stokes seed to

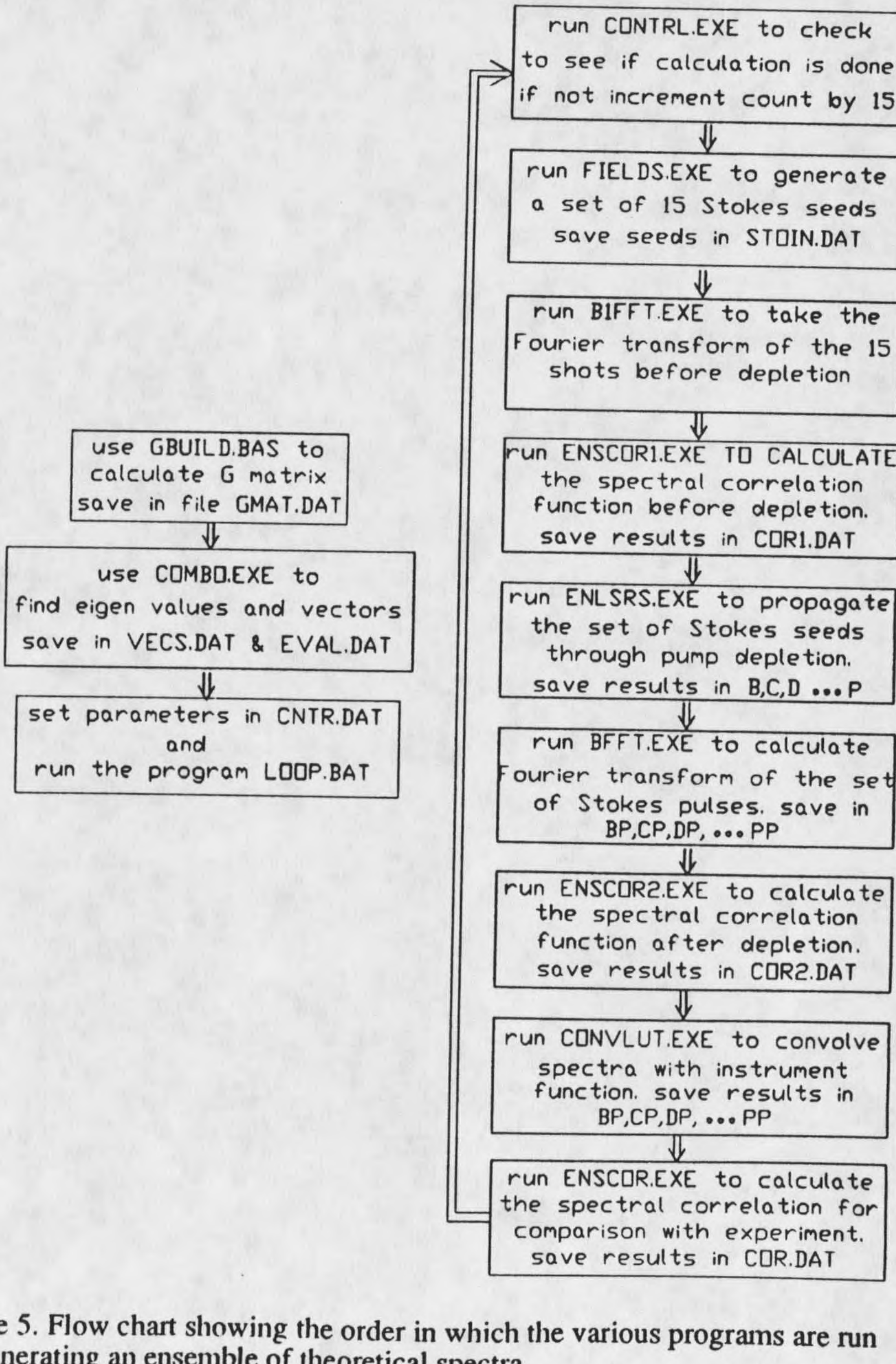

Figure 5. Flow chart showing the order in which the various programs are run for generating an ensemble of theoretical spectra.

produce a member of the ensemble after depletion. The ensemble average intensity of the Stokes seed was scaled to be approximately 1% of the pump intensity. This insured that the modes had not yet begun to compete for pump photons. However, at this energy the coherent modes have on the order of 10^{12} photons justifying the use of the semiclassical equations. The same pump pulse that was used to generate the coherent modes was used as the initial E_p for the depletion program. This leaves the length of the nonlinear region as the one remaining parameter to adjust. By comparing with the experimentally depleted temporal pump pulses, the gain distance was adjusted to give the observed amount of depletion or equivalently the correct Stokes pulse duration.

To perform the nonlinear calculation the program ENLSRS.FOR was used. The program is listed in Appendix B. The original version of this program was written by Kai Druhl and many modifications were made to adapt it to our needs. Figure 6 shows the retarded time frame coordinate system and the boundaries where the initial conditions are specified for the nonlinear integration. A program very similar to ENLSRS.FOR which is named NLSRS.FOR was used to perform the amplifier calculations which will be discussed in Chapter 5. For this case, the input fields were measured by splitting off a portion of the pump and Stokes pulses before they entered the amplifier.

The initial conditions are the pump and Stokes fields for the range of time of interest along the line z=0, and the polarization in the medium along the line $\tau = 0$. In Figure 6, a sketch of the input pump is shown along the line z=0 and the output pump is sketched along a line representing the end of the Raman medium. For our calculations, the initial polarization was set to zero along the line $\tau = 0$. The line $\tau = 0$ corresponds to the time just before the pump pulse arrives for all locations in the medium. Lines of constant t are represented by the diagonals in Figure 6. Information from the initial conditions along the solid line boundaries of the cross hatched region is propagated through the cross

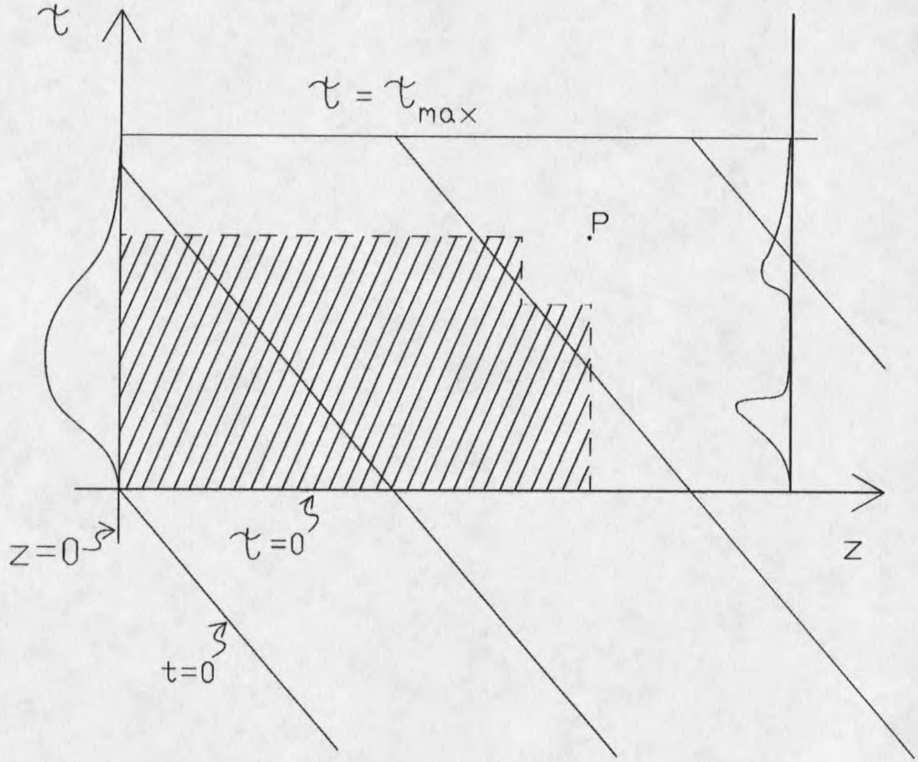

Figure 6 Retarded time coordinate system for the nonlinear integration. The diagonal lines are at constant t. The input and output pump envelope are sketched at the entrance and exit of the cell.

hatched region to the dashed line boundaries. The notch in the cross hatched region represents the step sizes dz and $d\tau$. Information from the three corners of the notch are used to calculate the fields and polarization at point P.

The integration algorithm is diagramed in Figure 7. The first part of the integration propagates the polarization (Q) up the z=0 axis. Physically, this corresponds to calculating the polarization in the first slice of the medium produced by the unchanged input fields. The value of the fields and polarization at z=0 and $\tau = 0$ are used to estimate the polarization at the half step point (1) and the full step point (2). Next the input fields and the estimated Q at point (2) are used to propagate Q from point (1) to point (2). Using this procedure an underestimate of Q during the first half step will be approximately canceled by an overestimate during the second half step and vice versa. This procedure is repeated to calculate Q at point (3) and the rest of the points along the τ axis.

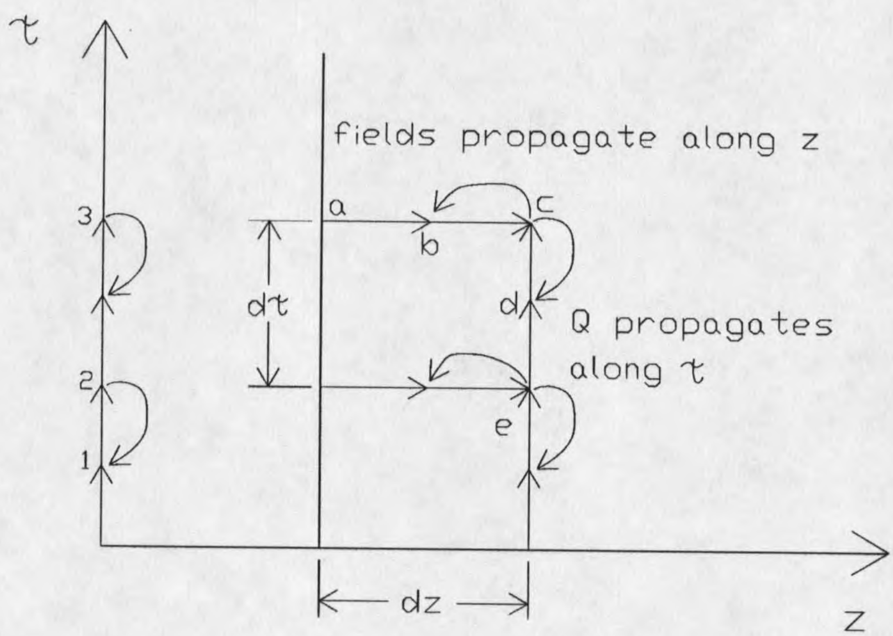

Figure 7 Diagram of the integration procedure. Error along the first half step is approximately canceled along the second half step.

Once Q has been determined along the τ axis, a second integration routine is used to propagate the fields through the medium to a larger z. To calculate the fields and Q at point (c), the value of the fields and Q at point (a) are used to first estimate the fields at points (b) and (c). Next the fields and Q at point (e) are used to estimate Q at points (d) and (c). The estimated value of Q at (c) is then used to propagate the fields from (b) to (c). The resulting fields at (c) are then used to propagate Q from (d) to (c). We have found that this routine is very reliable as long as the time step is short compared to the coherence time of the medium and the z stepsize is short compared to the e folding length of the fields. For the soliton calculations, the temporal stepsize had to be made quite short due to the rapid change in the fields. In fact, for the 100 atmosphere calculations, the temporal stepsize was continually adjusted by the computer so that the points were dense in the soliton region.

The input parameters for the program NLSRS.FOR are saved in the data files PULSE.DAT and AUTO.DAT. The parameters that need to be specified are:

Raman linewidth in rad/sec HWHM

Raman gain or equivalently the length of the nonlinear region

Scale factors for the pump and Stokes pulses

Time range over which to do the calculation

Step size in time

Step size in space

File names for the input and output fields

Effective detuning Δ_e

Once these parameters are set, the program will propagate a set of 15 Stokes seeds through pump depletion. A fast Fourier transform program named BFFT.FOR is used to calculate the energy spectrum from the resulting set of 15 temporal pulses. The output of the transform is expressed in GHz because the input temporal data is expressed in nanoseconds. The program uses frequency and not rad/sec.

In order to compare the theoretical spectral results with experimental data, the frequency resolution of the Fabry Perot interferometer must be taken into account. This is done by performing a convolution of the instrument function with the theoretical data. The energy spectrum after convolution, $U(\nu)$, is computed from the initial energy spectrum, $U'(\nu)$, using

$$U(\nu) = \int_{-\infty}^{+\infty} U'(\nu') \frac{d\nu'}{1 + (2F/\pi)^2 \sin^2[(\nu - \nu')/2]} \tag{3.18}$$

where F is the finesse or resolution of the Fabry Perot interferometer. Experimentally, the finesse of the interferometer that was used to measure the Stokes spectrum was determined by using a helium neon laser. When measuring the finesse, mirrors were used which had specifications at the helium neon wavelength which were identical to those for the Stokes mirrors at the Stokes wavelength. The measured finesse using the helium neon laser was 75 which is the number that was used in the convolution program.

Theoretical Results

The first test of the theory was to see if the energy spectrum of individual shots had qualitatively the same shot to shot variations as those observed experimentally. The single shot experimental data will be presented in the next chapter. Two examples of the theoretically generated Stokes energy spectrum are shown in Figures 8 and 9. When the spectra from 300 members of the ensemble were averaged together, the expected gain narrowed linewidth was recovered. The gain narrowed linewidth is shown as the dashed curve in Figures 8 and 9. As will be shown later, experimental shots can be found which look qualitatively like those from theory. For some shots, the spectrum consists of predominantly one peak like that shown in Figure 8. For other shots the spectrum has multiple peaked structure like that shown in Figure 9. It appears that given a theoretically

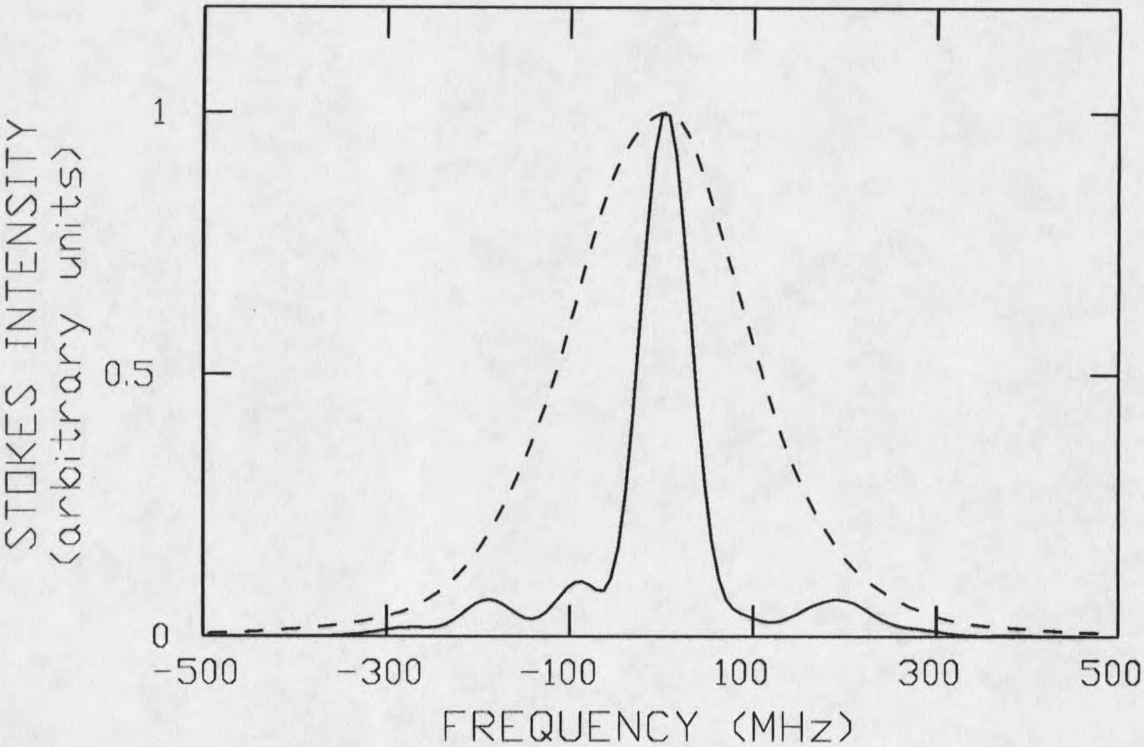

Figure 8 Theoretically generated sample of a single shot Stokes spectra. The theory can generate near transform limited pulses which are much narrower than the ensemble average.

generated spectrum, a similar experimentally generated spectrum can be found with approximately the same shape if one looks through enough shots. The width of the spectrum shown in Figure 8 is much narrower than the average linewidth. In fact it is nearly transform limited which means that the pulse had minimal phase variations under the pulse envelope. The characteristic width of the spectral peaks is given by the Fourier transform of the temporal pulse envelope.

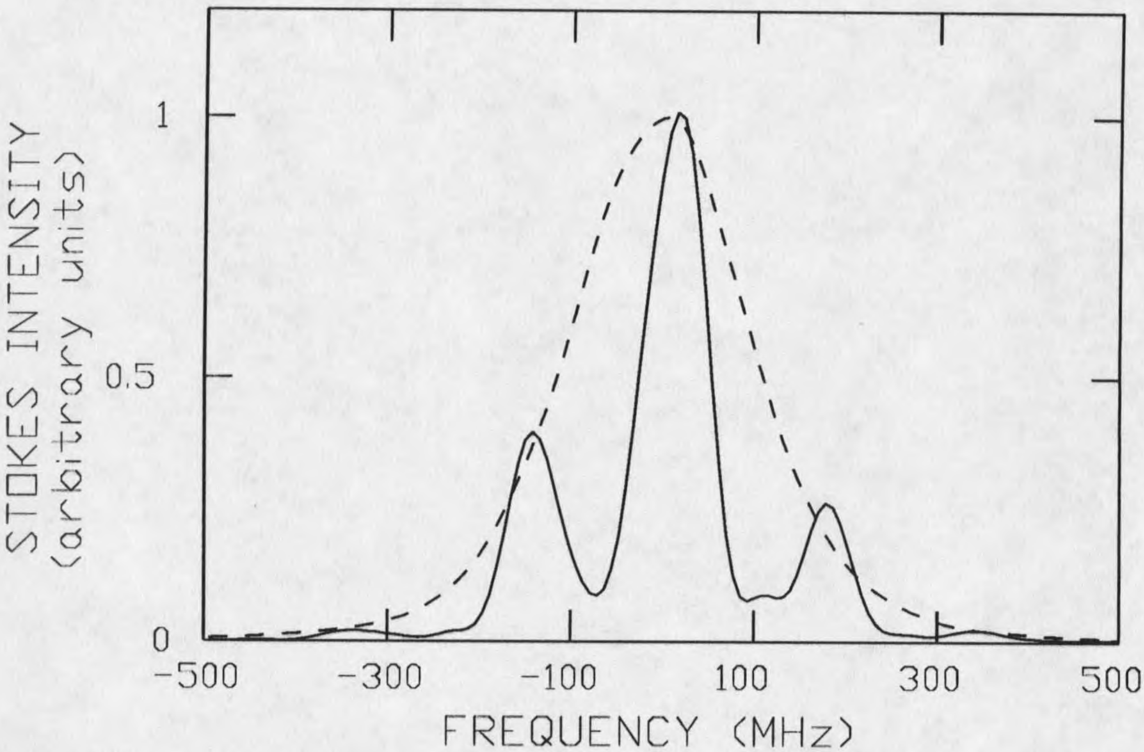

Figure 9 Example of a theoretically generated single shot Stokes spectra with multiple spikes. When an ensemble of spectra are added together, the gain narrowed line shape is obtained.

The gain narrowed linewidth is determined by the average linewidth of the Stokes field in the quantum initiation region and the total gain that this spontaneously emitted light experiences as it is amplified by stimulated emission. Spectral components which are on resonance will experience more gain than those which are off resonance and thus the spectrum will narrow. The ratio of the linewidth after gain narrowing to that of the spontaneous emission is given by[14]

$$W_F/W_I = \sqrt{\ln(2)/\ln(P_F/P_I)} = \sqrt{\ln(2)/gz} \tag{3.19}$$

where P_I and P_F are the initial and final Stokes powers and gz is the Raman gain times the length of the medium. Note that this gain narrowing factor is very insensitive to the measured final Stokes power. For example, a factor of two uncertainty in the final power leads to a 1% uncertainty in the narrowing factor. Using an initial Stokes power of $P_I = \hbar\omega\Gamma/2$ which corresponds to one half of a photon per mode weighted by the Raman linewidth, the gain narrowing factor in our experiment was predicted to be 1/6.85 resulting in a gain narrowed linewidth of 219MHz at 32atm. The gain narrowed linewidth will be discussed further in Chapter 5 in the section on soliton decay.

In order to make a quantitative comparison with experiment, the two frequency spectral correlation function was calculated using the set of 300 theoretically generated ensemble members. The spectral correlation function is defined by

$$C(\Delta\nu) = \langle \int_{-\infty}^{+\infty} U(\nu + \Delta\nu) U(\nu) d\nu \rangle \tag{3.20}$$

where $U(\nu)$ is the single shot energy spectrum and the brackets denote an average over the ensemble. Computer programs named ENSCOR1.BAS, ENSCOR2.BAS, and ENSCOR.BAS were used to calculate the spectral correlation function before depletion, after depletion, and after convolution respectively. A comparison with the experimentally measured spectral correlation function will be made in Chapter 4. Experimentally, only the spectral correlation after convolution with the Fabry Perot instrument can be easily observed. However, the other theoretical correlation functions give insight into the amplification process. The theoretically generated spectral correlation function before and after convolution with the Fabry Perot instrument function are presented in Figure 10. As will be discussed in Chapter 4, the theoretically generated spectral correlation function agrees quite well with experiment. The features of the correlation function will be discussed in the next section.

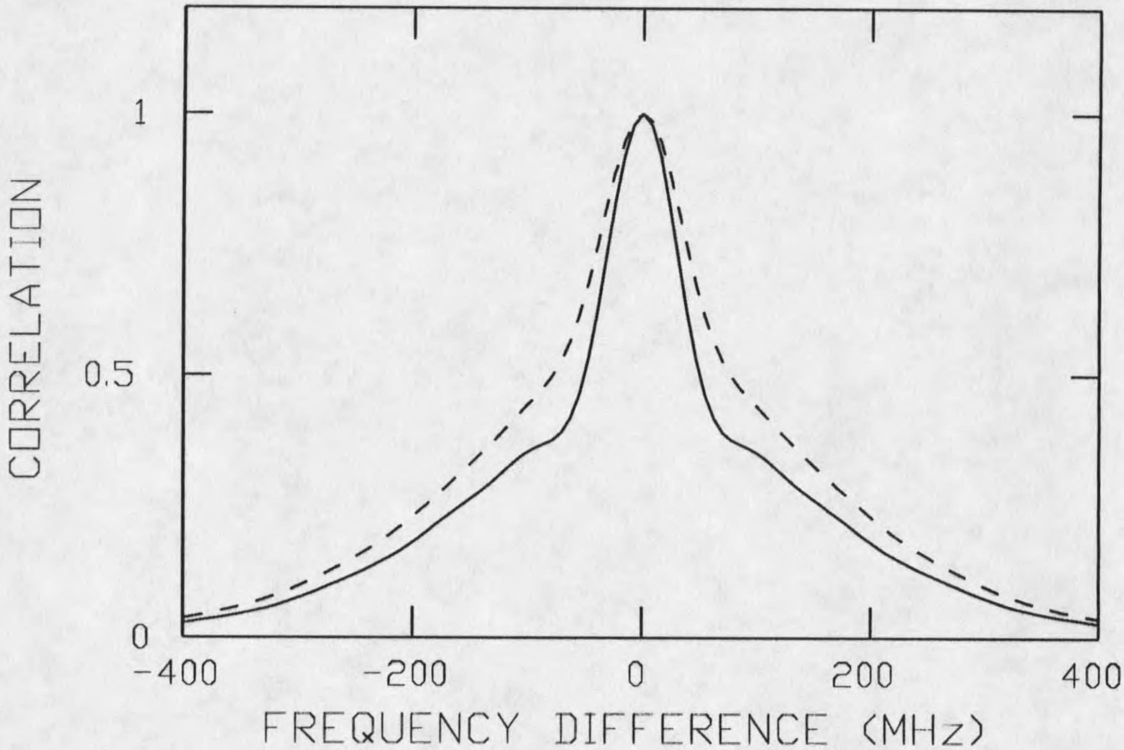

Figure 10 Autocorrelation calculated from coherent modes theory with infinite instrument resolution (solid curve) and with a Fabry Perot resolution of 14.3MHz FWHM (dashed curve). The instrument resolution obscures the shoulder which is generated in the nonlinear regime. The dashed curve is also shown in Chapter 4 for comparison with experiment.

Discussion on Propagation Through Depletion

At this point, the theory appears sufficient to explain the experimental observations. In addition, the theory gives some insight into how the power spectrum evolves through depletion. At this time, we are not able to observe experimentally the amplification through depletion due to the weak intensities. To investigate the propagation of the fields through depletion, two sets of Stokes seed ensembles were used. The first set was generated from coherent modes by adding together the 15 largest statistically weighted modes. The second set was made up from the 3 largest modes. The set using 15 modes gives a slightly better and presumably correct result.

First results before and after depletion using 15 modes to generate a 300 member ensemble will be presented. Figure 11 shows the results for the average linewidth.

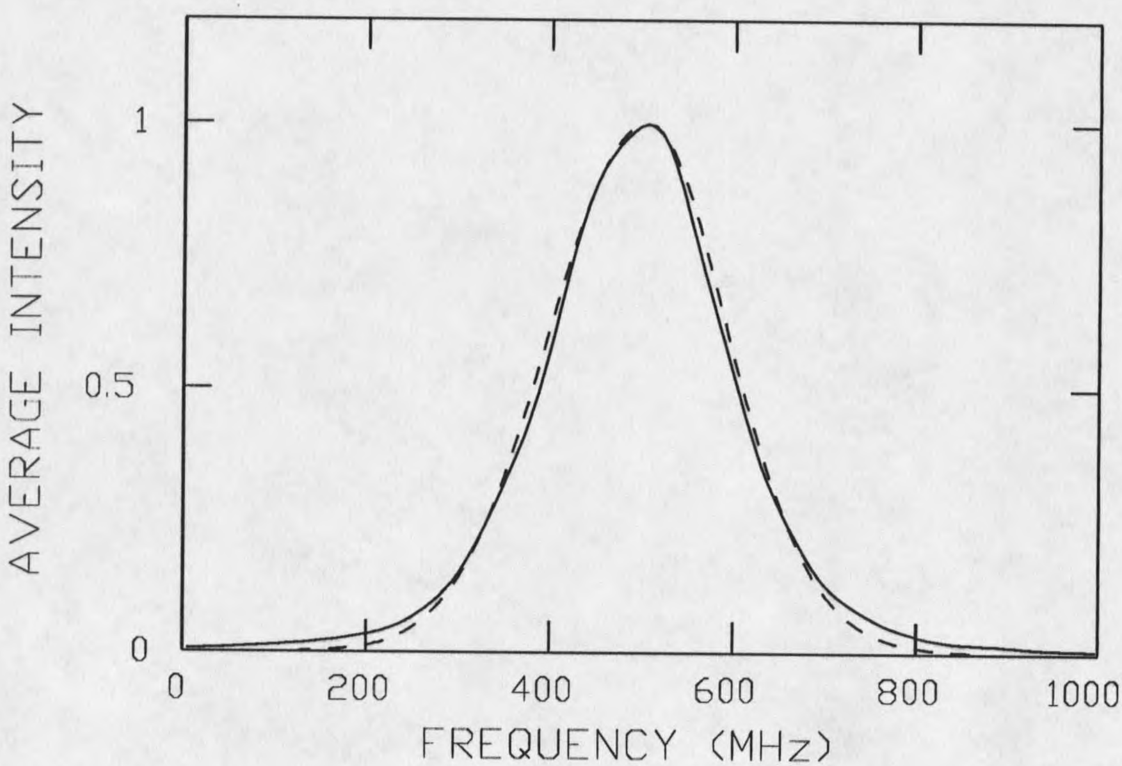

Figure 11 Ensemble average power spectrum calculated using 15 temporal modes for 300 ensemble members before pump depletion (dashed curve) and after pump depletion (solid curve). Pump depletion leaves the average linewidth unchanged as the uncorrelated wings of the Stokes pulse are amplified.